MAGNETOM Flash

The Magazine of MRI

SIEMENS

MR Neurography

50

Avneesh Chhabra, M.D.
Assistant Professor

Radiology and
Orthopedic Surgery

The Russel H. Morgan
Department of Radiology
and Radiological Science

Johns Hopkins University
School of Medicine
Baltimore, Maryland, USA

Dear Reader,

I am pleased to edit this exciting MAGNETOM Flash issue on Magnetic Resonance Neurography (MRN). Incorporation in the RSNA edition of the magazine also makes it special as it will have a wider audience and multi-specialty reach.

This edition has three articles covering different aspects of the peripheral nervous system from spinal cord to peripheral nerves. Latest 2D and 3D techniques in practice and future directions in both anatomic and functional domains of peripheral nerve imaging are addressed in detail.
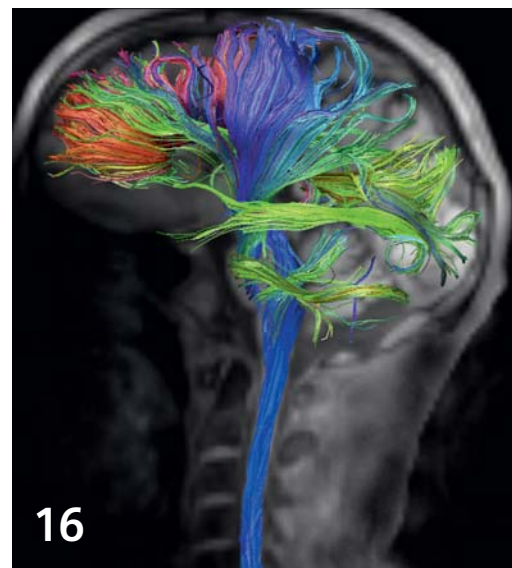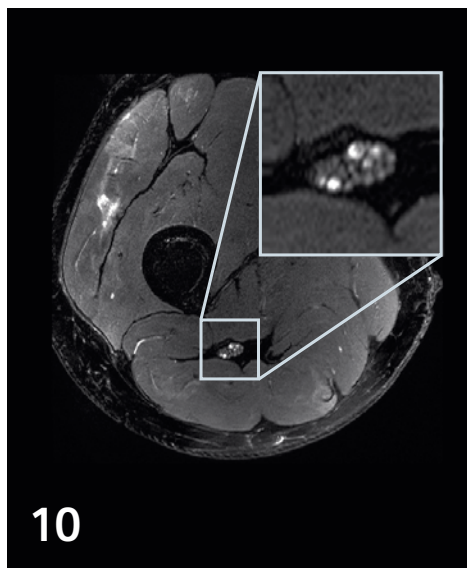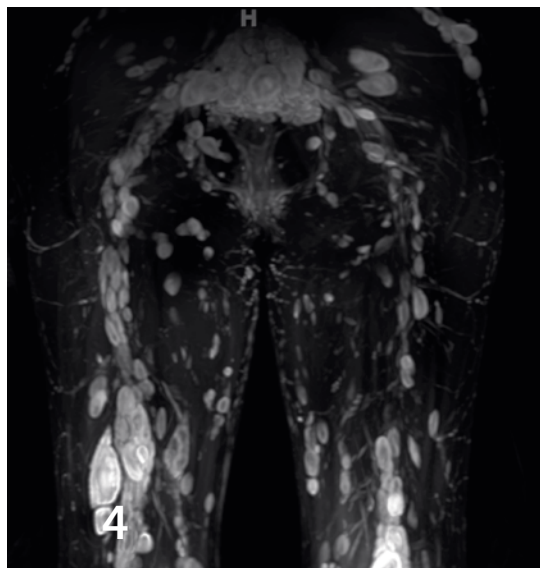
Current high field technology depicts high resolution intra-neural fascicular detail in both normal and abnormal states as described in the article by Philipp Bäumer et al. (Heidelberg University Hospital, Germany). The high resolution imaging is important for diagnosis and surgical planning of nerve injuries, entrapments and for further evaluation of diffuse or polyneuropathies. Various technological developments, interpretation criteria, and future directions towards technique improvement are highlighted in my article from the work I have performed at Johns Hopkins University Hospital. Finally, there is an important article on diffusion tensor imaging improvement using *syngo* RESOLVE technique for functional spinal cord and brain imaging.

A bright future lies ahead for MRN with rapid deployment of this technology in current clinical setting for a variety of neuropathy diagnoses encompassing referrals from a number of providers, including neurosurgeons, neurologists, peripheral nerve surgeons, hand or foot and ankle specialists, plastic surgeons, and rehabilitation specialists. We will see further improvements in coming years in both anatomic and functional techniques, while user friendly analytic software becomes available.

Please enjoy reading the latest and inspiring RSNA issue of MAGNETOM Flash!

Avneesh Chhabra, M.D.

4

10

16

MR Neurography

Magnetic Resonance Neurography – Techniques and Interpretation

Avneesh Chhabra, M.D.[1]; Abraham Padua Jr., Ph.D.[2]; Aaron Flammang, MBA[2]; Wesley Gilson, Ph.D.[2]; John A. Carrino, M.D., M.P.H.[1]

[1]Department of Radiology & Radiological Science, Johns Hopkins University, Baltimore, MD, USA
[2]Siemens Healthcare, Malvern, PA, USA and Erlangen, Germany

Introduction

Magnetic resonance neurography (MRN), akin to angiography, is an ever-advancing technology for multiplanar depiction of normal and abnormal peripheral nerves. This article will highlight various 2D and 3D pulse sequences available for non-selective and selective nerve visualization as well as their functional evaluation. Related interpretation pearls and pitfalls are discussed.

Techniques

MRN is best performed on 3 Tesla (T) scanners with dedicated extremity or wrap around flex coils as they can provide higher signal-to-noise ratio (SNR), which is essential to enhance the smallest structure in the neurovascular bundle, namely the peripheral nerves [1].

On current 1.5T scanners (MAGNETOM Aera, MAGNETOM Avanto), 2D (dimensional) imaging can be performed with near-similar resolution as on 3T scanners, however 3D imaging is often limited, especially if smaller voxels are used or fat suppression is applied. On the other hand, if there is metal in the field-of-view, in order to mitigate susceptibility artifacts and for superior nerve visualization, 1.5T imaging is often favored.
2D pulse sequences include high resolution (base resolution 256 or higher, in plane resolution 0.3–0.4 mm) T1-weighted and fat suppressed T2w images. Uniform fat suppression is essential to avoid artifactual increase in nerve signal intensity. Options include frequency selective fat suppression

(fsT2w), short tau inversion recovery (STIR), and spectral adiabatic inversion recovery (SPAIR), or 2-point or 3-point Dixon techniques. fsT2w is often limited due to loss of fat saturation along the curvatures of extremities, especially in large subjects. STIR works well for 3D imaging with excellent fat suppression, however for 2D imaging it is often marred by poor SNR, excessive SAR (specific absorption rate) deposition and pulsation artifacts. SPAIR works well as it provides better fat suppression than fsT2w and higher SNR than STIR. It has virtually no pulsation artifacts and is also relatively SAR favorable (Fig. 1). It comes in weak and strong contrast versions. The authors prefer the strong version as it provides isointense signal in normal nerves [2].
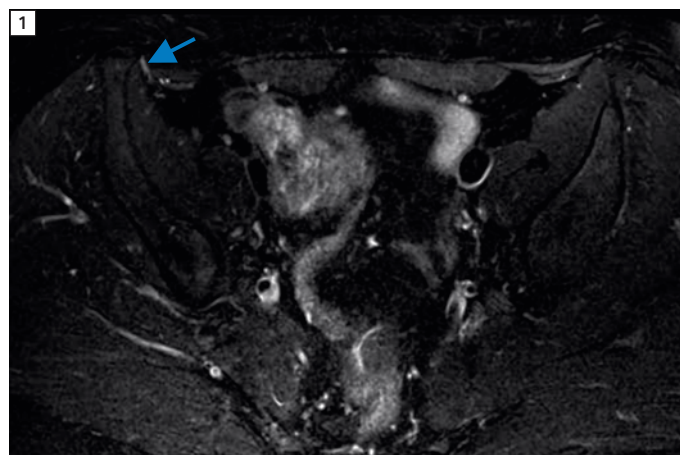
1 Meralgia Paresthetica. Young woman with right anterolateral thigh pain and suspected lateral femoral cutaneous (LFCN) nerve abnormality. Axial T2 SPAIR image shows uniform fat suppression and abnormally hyperintense right LFCN (arrow) in keeping with clinical diagnosis of meralgia paresthetica.
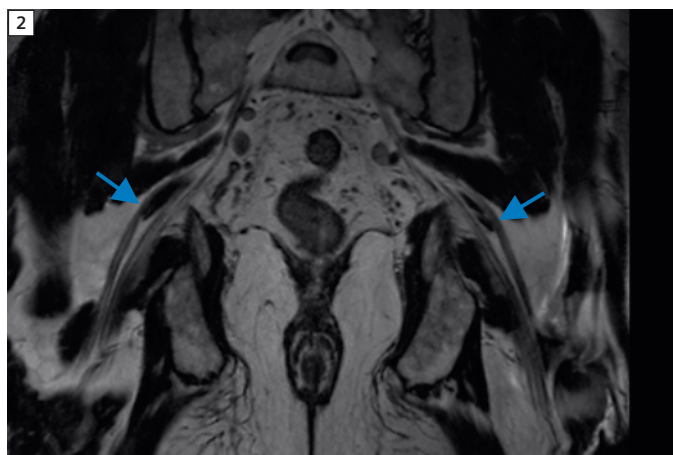
2 T2 SPACE. Coronal non-fat suppressed T2 SPACE image through the pelvis shows bilaterally split sciatic nerves (arrows) in this patient with no symptoms of sciatica.

Dixon technique applied with T2w imaging gives separate water and fat images and also provides excellent fat suppression with higher SNR and contrast-to-noise ratio than STIR or SPAIR.

3D pulse sequences can be divided into anatomic and functional techniques. Anatomic techniques are further divided into nerve non-selective and nerve selective sequences. Nerve non-selective techniques include T1w imaging, namely VIBE (volume interpolated breathhold examination, T1 3DGRE) or MPRAGE (3D GRE); and T2w multislab acquisition, namely SPACE (sampling perfection with application optimized contrasts using varying flip angle evolutions) [3]. SPACE is heavily used in MRN examinations as isotropic spine echo type imaging can obtained using SPACE in a variety of contrasts (T1, PD, T2, STIR, and SPAIR) with constant or variable echo times (Fig. 2). The authors use VIBE for pre- and post-contrast imaging, and otherwise mostly use 3D imaging with fluid sensitive contrast. 3D STIR SPACE provides best fat suppression for the brachial and LS plexus while 3D SPAIR SPACE provides higher SNR along with good fat suppression for extremity imaging (Figs. 3, 4). Dixon T2w imaging also provides excellent images of the brachial plexus, however currently can be acquired in 2D mode only (Fig. 5). Others such as 3D PD SPACE with variable echo time can produce similar image quality and allows multiplanar reconstruction (Fig. 6). Currently, 3D STIR SPACE and SPAIR SPACE sequences are most widely used and are time tested. Maximum intensity projections (MIP) of acquired images or their curved planar reformats produce excellent quality nerve images along their long axis. It remains to be seen if other techniques, such as Dixon with SPACE, can be obtained within acceptable time periods and provide the necessary isotropic spatial and good contrast resolution.

3D nerve selective imaging includes diffusion-weighting (DW) with a small b-value ($80–200$ s/mm^2) to suppress flowing blood. It is a fine balance as one adds diffusion gradient to the 3D imaging, as it reduces SNR and can degrade image quality while providing the benefit of vascular flow signal suppression for selec-
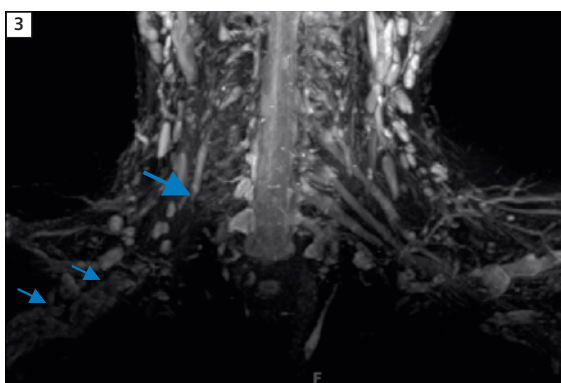
3 3D STIR SPACE. 24-year-old man with recent motor vehicle accident and flail right arm. MIP image from coronal 3D STIR SPACE sequence shows transected right L5 nerve (large arrow). Notice torn, retracted and bunched up remaining right brachial plexus (small arrows).
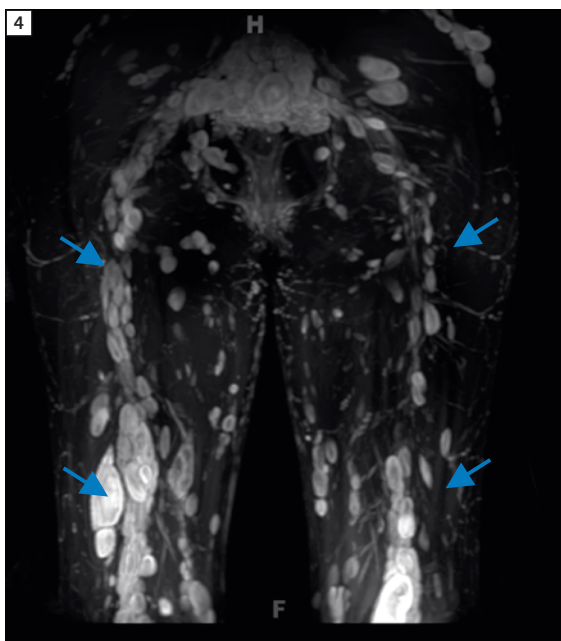
4 SPAIR SPACE. MIP image from coronal 3D SPAIR SPACE sequence shows multifocal nodular enlargement of bilateral sciatic nerves, infiltrated by numerous neurofibromas (arrows) in this known case of NF type I.
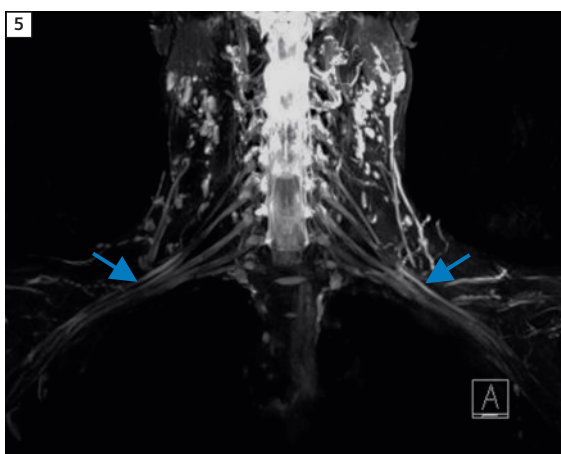
5 T2 Dixon. MIP image from coronal 2D T2 Dixon sequence shows excellent depiction of normal bilateral brachial plexuses (arrows) in a healthy volunteer.
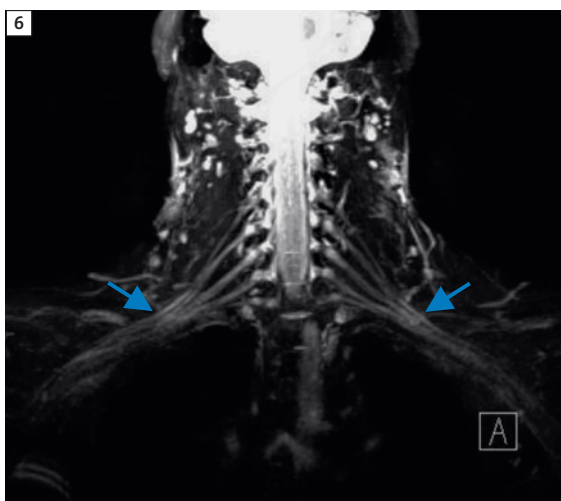
6 PD variable 3D SPACE. MIP image from coronal PD variable 3D SPACE sequence shows excellent depiction of normal bilateral brachial plexuses (arrows) in a healthy volunteer.

7 3D DW PSIF. Young woman with persistent carpal tunnel symptoms following a prior transverse carpal ligament release. Notice normal median (large arrow) and ulnar nerves (medium arrow) proximal to the carpal tunnel. A neuroma in continuity is seen along the distal aspect of the carpal tunnel (smallest arrow). Notice selective nerve depiction with excellent vascular signal suppression
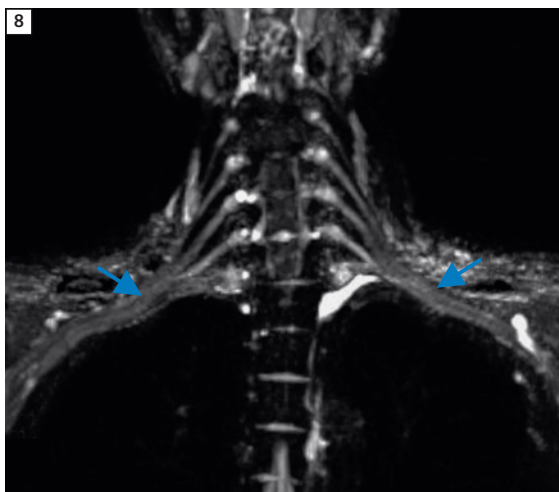
8 3D DW SPACE. MIP image from coronal DW 3D STIR SPACE sequence shows selective depiction of normal bilateral brachial plexuses (arrows) in a healthy volunteer. However note decreased SNR due to added diffusion component.
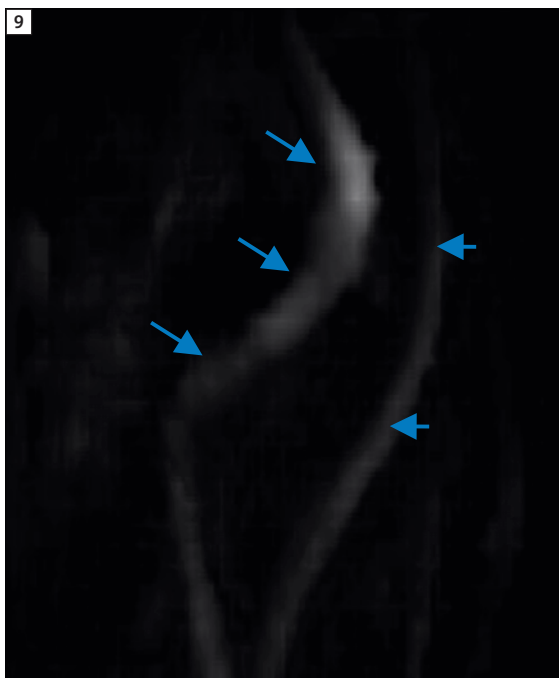
9 DTI. MIP coronal tensor image with inverted grey scale from axial DTI sequence shows enlarged ulnar nerve with abnormally low FA and high ADC values in this case of re-entrapped ulnar nerve at the site of prior anterior transposition (large arrows). Notice normal median nerve (small arrows).

tive nerve imaging. The sequences include 3D DW PSIF (reversed steady state free precession) and DW STIR SPACE. 3D DW PSIF is very susceptible to local inhomogeneity, motion artifacts, breathing artifacts, and poor fat suppression. Water selective fat suppression currently works well with PSIF [4, 5]. With appropriate technique, it provides excellent nerve selective images (Fig. 7). MIP images from DW PSIF and DW SPACE provide good nerve selective depiction (Fig. 8). With further pulse sequence development, one can look at adding Dixon to DW PSIF or try to improve DW SPACE sequence that can be obtained in acceptable time periods while keep the advantages of nerve selectivity. A typical lumbosacral plexus protocol has been highlighted in Table 1. Normal nerves do not enhance as they are outside the blood-nerve barrier. Contrast imaging (gadolinium based agent) does not add much in trauma or entrapment neuropathy cases as these are mostly subacute cases. In these cases, only denervated muscles enhance, the demonstration of which is already visible on T1w and fat suppressed fluid sensitive images. Contrast administration is, however, recommended in other cases, such as suspected neural and perineural mass lesions, polyneuropathy conditions including lymphoma, amyloidosis, demyelinating neuropathies, hereditary neuropathies, etc.

Functional imaging of the peripheral nerves primarily includes diffusion tensor imaging (DTI). It has been exploited in various extremity and plexus peripheral nerves in the last few years and continuous refinements are being made. Single shot echo planar imaging (EPI) is the technique used in most centers and multiple diffusion moments (b-values) are applied to obtain functional parameter of apparent diffusion coefficient (ADC) [6]. At least 6 directions of interrogation are needed for DTI, although most authors have used 12–20 directions to obtain reproducible data. The authors use 3 diffusion moments (0, 800, 1000 s/mm²) and 12 directions of interrogation. Tight echo spacing, frequency selective fat suppression, auto-shimming before image acquisition and no motion degradation
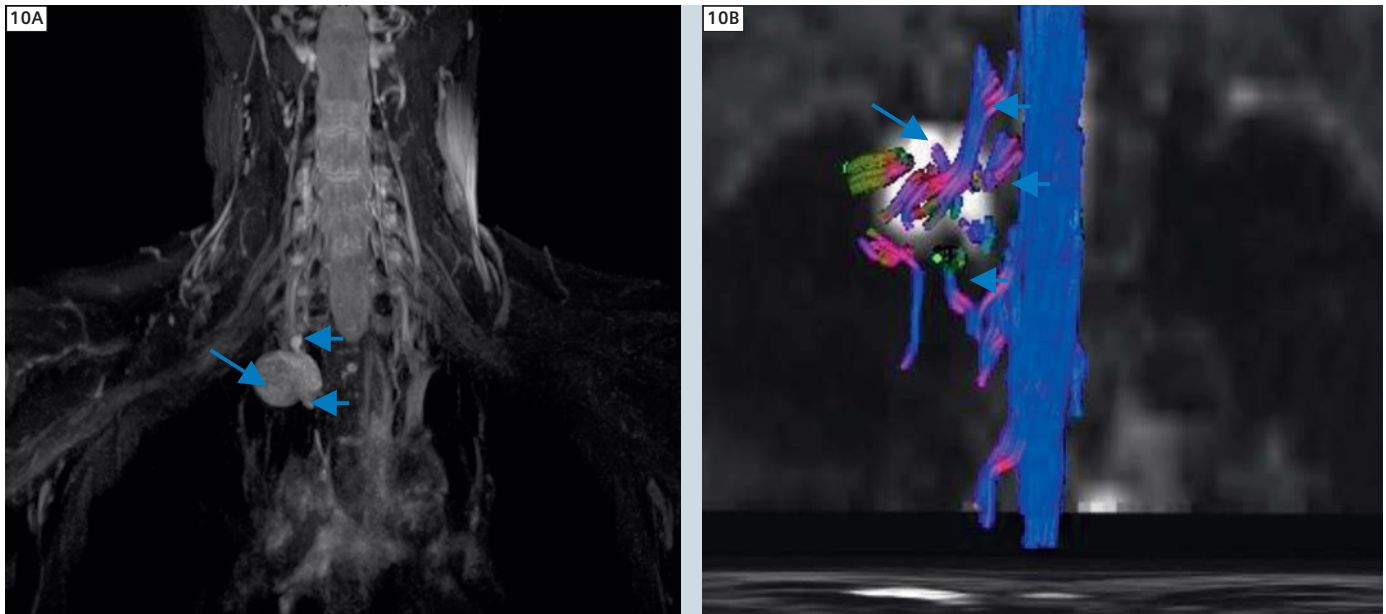
10 3D STIR SPACE and DTI. MIP image from coronal 3D STIR SPACE sequence **(10A)** shows normal depiction of normal bilateral brachial plexuses in a 39-year-old woman with incidentally detected lesion on chest CT (not shown). A peripheral nerve sheath tumor (large arrow) is nicely depicted in close relation to paraspinal T1 and T2 ganglia (small arrows). The lesion showed high ADC values in keeping with a benign lesion. Tractography image from DTI **(10B)** shows the nerve roots (small arrows) draped over the lesion (large arrow) without involvement.

Table 1: The imaging protocol employed in the magnetic resonance neurography examination for the LS plexus.

MR sequence	Slice thickness (mm)	TR / TE (ms)	TF	Base resolution (pixels)
Axial T1	4	800 / 12	6	832
Coronal T1	4	960 / 12	5	384
Axial T2 SPAIR	4	4890 / 80	22	256
Sagittal T2 3D SPACE	1	1000 / 97	81	256
Sagittal STIR	4	3700 / 18	22	256
Coronal STIR 3D SPACE	1.5	1500 / 91	41	256

are essential to obtain good and reproducible DTI data. Axial images obtained with 4–5 mm slice thickness with 0 gap can be reconstructed in multiple planes without artifacts (Fig. 9). These images then allow accurate tensor calculation, fractional anisotropy (FA) measurements and tractography. DTI has proven useful in non-invasive pre- and post-operative evaluation of carpal tunnel syndrome patients and peripheral nerve sheath tumors (PNST) as the involved nerves show reduced FA values that improve over time with treatment [7]. The benign PNSTs show higher ADC values than their malignant counterparts and tractography differences exist among different tumor types depending upon internal fascicular involvement or mere displacement [8] (Fig. 10). Further investigations are underway to evaluate the role of DTI in other types of neuropathies.

Interpretation pearls and pitfalls

While image generation is getting easier with high field MR techniques, the radiologists should learn to correctly interpret these high quality examinations. There is a steep learning curve for those who spend time with attention to detail, since nerve architecture is easily visible to the fascicular and perineurium level. One should learn normal nerve anatomy, variations, diagnostic pearls and pitfalls while obtaining all the information possible from clinical findings and available electrodiagnostic test results. Electrodiagnostic tests are also limited by false negative or indeterminate results, especially in deeply located nerves. So, while these results are helpful, one

should not get biased by negative results. The reader should follow a step-wise approach to imaging diagnosis:

1. Image quality – is it adequate and is fat suppression uniform? Are the nerves visible adequately and can the nerves be separately evaluated from adjacent vessels or compared side to side if the contralateral portion of body is available, such as in pelvic imaging. Recognize normal nerves and their variations (bifid nerve, split nerve with muscle belly intervening, intramuscular course of the nerve, etc.)

2. Look for orthopedic internal derangements which can mimic similar neuropathic symptoms or are potential cause of traction neuropathy, such as spondylosis, plantar fasciitis, tibialis posterior dysfunction, etc.

3. Look for clues of disseminated or systemic causes of neuropathy: one nerve abnormal over long distance away from entrapment sites or multiple regional nerves abnormal. This may happen in diabetic neuropathy, demyelinating neuropathies, hereditary neuropathy, vasculitis or toxic metabolic conditions. Usually hereditary neuropathy results in symmetric disease as compared to acquired conditions. Clinical findings should be correlated for insights into above diagnoses.

4. Look for focal area of nerve abnormality, abnormal T2 hyperintensity (approaching adjacent venous signal intensity) and / or fascicular abnormality (enlargement / effacement from edema / discontinuity) indicating entrapment or injury in the correct clinical scenario. If the nerve is really abnormal, the signal intensity will persist over few to many sections along its length versus signal change from a magic angle artifact. The nerve further enlarges with worsening neuropathy forming a pseudoneuroma in entrapment and neuroma in injury (lost partial or complete fascicular continuity with heterogeneous appearance) [9]. The nerve abnormality is generally worst at the site of insult and it fades gradually proximally and distally. Abrupt change in nerve intensity from bright-black-bright signal (Triple B sign) usually means severe focal neuropathy and a potential surgical case. Painful neuroma in continuity and nerve discontinuity in functionally important nerves also require surgical repair/reconstruction. Long standing neuropathy, such as in diabetes, can lead to atrophic appearance of the nerve with fascicular atrophy and intra-epineurial fatty proliferation / replacement.

5. Evaluate regional muscles. As a rule, the muscle denervation changes are distal to the site of insult. If muscle changes are patchy or widespread in different nerve territories or associated with fascial edema, the diagnosis could be myopathy / myositis rather than denervation change. The diagnosis can be made with confidence if regional nerves are normal.

6. In case of a mass lesion, further characterize the lesion into neural or perineural masses. Age, clinical findings and anatomic MRN plus DTI are useful in the imaging evaluation of neural masses. Perineural lesions are further evaluated based on anatomic imaging and contrast evaluation into lipoma, ganglion cyst, hematoma, and abscess etc.

7. Finally, look for prior local surgical changes or nerve repair/reconstruction changes. The signal alteration may persist but in successful cases, the signal decreases within the nerves and denervation changes in the muscle resolve. In worsening nerve degeneration cases, the nerve signal approaches fluid signal and persists till the nerve atrophy starts, while the regional muscles undergo continued fatty replacement and atrophy [10]. Correlation with prior imaging studies is essential in these cases.

To conclude, magnetic resonance neurography is an exciting imaging technique that affords multiplanar anatomic and functional depiction of peripheral nerves and their related lesions. Appropriate imaging and accurate interpretation are essential components of successful performance of this ever advancing technique.

References

1 Chhabra A, Lee PP, Bizzell C, Soldatos T. 3 Tesla MR neurography-technique, interpretation, and pitfalls. Skeletal Radiol 2011; 40:1249-1260.

2 Chhabra A, Andreisek G, Soldatos T, et al. MR neurography: past, present, and future. AJR Am J Roentgenol 2011; 197:583-591.

3 Vargas MI, Viallon M, Nguyen D, Beaulieu JY, Delavelle J, Becker M. New approaches in imaging of the brachial plexus. Eur J Radiol. 2010 May;74(2):403-10.

4 Zhang Z, Song L, Meng Q, et al. Morphological analysis in patients with sciatica: a magnetic resonance imaging study using three-dimensional high-resolution diffusion-weighted magnetic resonance neurography techniques. Spine (Phila Pa 1976) 2009; 34:E245-250.

5 Chhabra A, Soldatos T, Subhawong TK, Machado AJ, Thawait SK, Wang KC, Padua A Jr, Flammang AJ, Williams EH, Carrino JA. The application of three-dimensional diffusion-weighted PSIF technique in peripheral nerve imaging of the distal extremities. J Magn Reson Imaging. 2011 Oct;34(4):962-7.

6 Viallon M, Vargas MI, Jlassi H, Lovblad KO, Delavelle J. High-resolution and functional magnetic resonance imaging of the brachial plexus using an isotropic 3D T2 STIR (Short Term Inversion Recovery) SPACE sequence and diffusion tensor imaging. Eur Radiol 2008; 18:1018-1023.

7 Guggenberger R, Eppenberger P, Markovic D, Nanz D, Chhabra A, Pruessmann KP, Andreisek G. MR neurography of the median nerve at 3.0T: Optimization of diffusion tensor imaging and fiber tractography. Eur J Radiol. 2012 Apr 19. [Epub ahead of print]

8 Chhabra A, Thakkar RS, Gustav A et al. Anatomic MR imaging and functional diffusion tensor imaging of peripheral nerve tumor and tumor like conditions. AJNR 2012 (in press).

9 Chhabra A, Williams EH, Wang KC, Dellon AL, Carrino JA. MR neurography of neuromas related to nerve injury and entrapment with surgical correlation. AJNR Am J Neuroradiol; 31:1363-1368.

10 Chhabra A, Subhawong TK, Williams EH, Wang KC, Hashemi S, Thawait SK, Carrino JA. High-resolution MR neurography: evaluation before repeat tarsal tunnel surgery. AJR Am J Roentgenol. 2011 Jul;197(1):175-83.

Contact
Avneesh Chhabra, M.D.
Assistant Professor Radiology & Orthopedic Surgery
Russell H Morgan Department of Radiology & Radiological Science
Johns Hopkins University, Baltimore, MD USA
achhabr6@jhmi.edu

Missing information?
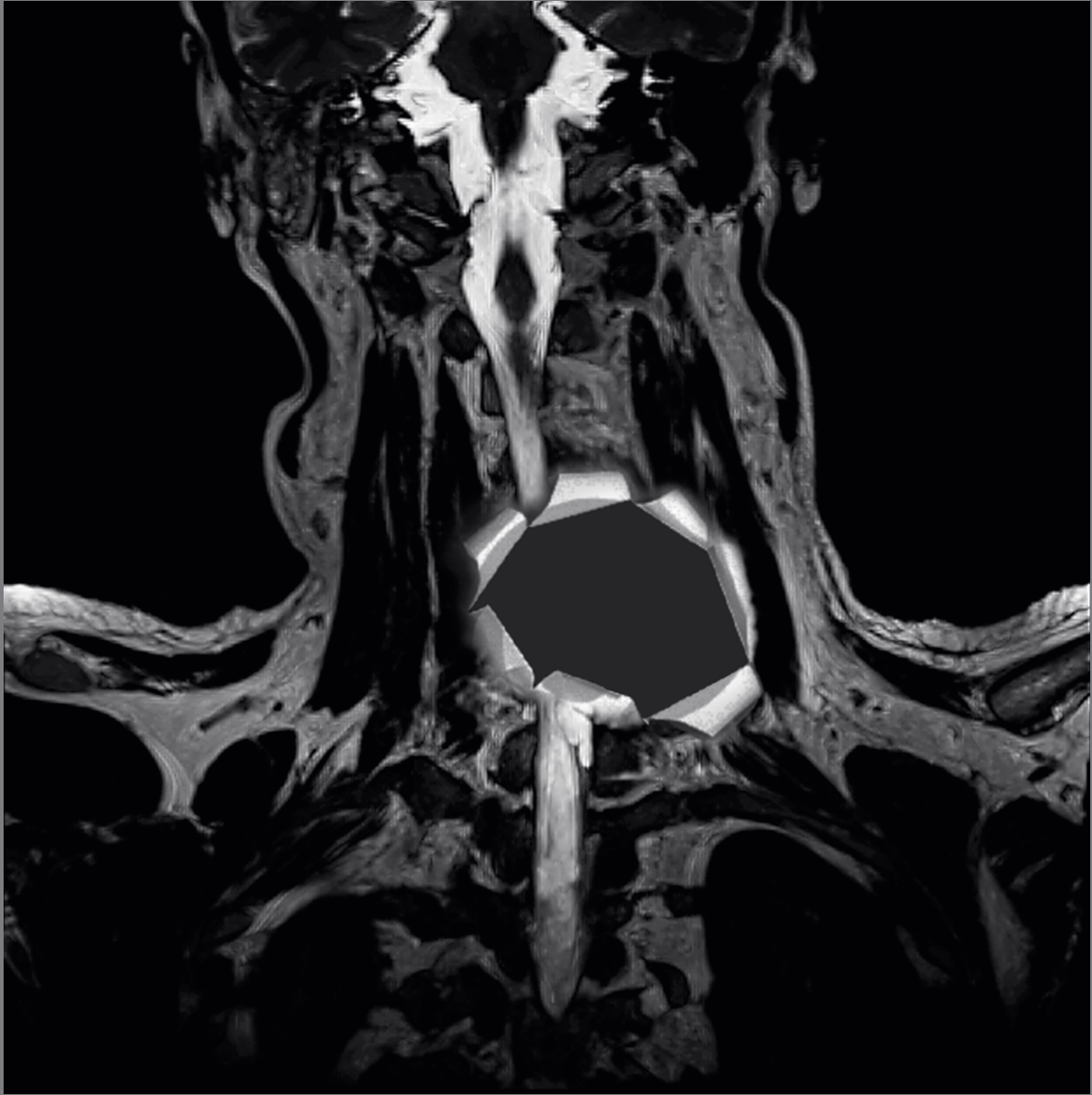
To make sure you have all the information you need, register for our free monthly newsletter on clinical MRI information. Check out case reports from MAGNETOM users around the world and stay up-to-date with Siemens software applications.

Register at
www.siemens.com/magnetom-world
Go to
Publications > Subscriptions

MR Neurography – Diagnostic Criteria to Determine Lesions of Peripheral Nerves

Philipp Bäumer, M.D., M.Sc.[1]; Sabine Heiland, Ph.D.[2]; Martin Bendszus, M.D.[1]; Mirko Pham, M.D.[1]

[1]Department of Neuroradiology, Heidelberg University Hospital, Germany
[2]Section of Experimental Radiology, Department of Neuroradiology, Heidelberg University Hospital, Germany

I) Introduction with potential clinical indications

Clinical examination and electrodiagnostic testing comprise the traditional methods of diagnostic investigation in peripheral nerve disease. These are excellent tools to assess function of peripheral nerves but can be limited in localizing a lesion. Recent developments in MR scanner and coil technology and the refinement of pulse sequences for increasing structural resolution have allowed imaging of fine details in healthy and diseased peripheral nerve [1, 2]. MR Neurography (MRN) at high magnetic field strength of 3 Tesla allows for the visualization of peripheral nerves at the fascicular level – the fascicle being the first order subunit of a peripheral nerve. The major limitation of clinical and electrophysiological examination is precisely the strength of MRN: the exact localization of nerve lesions. Lesion localization and spatial lesion patterns in the periph-
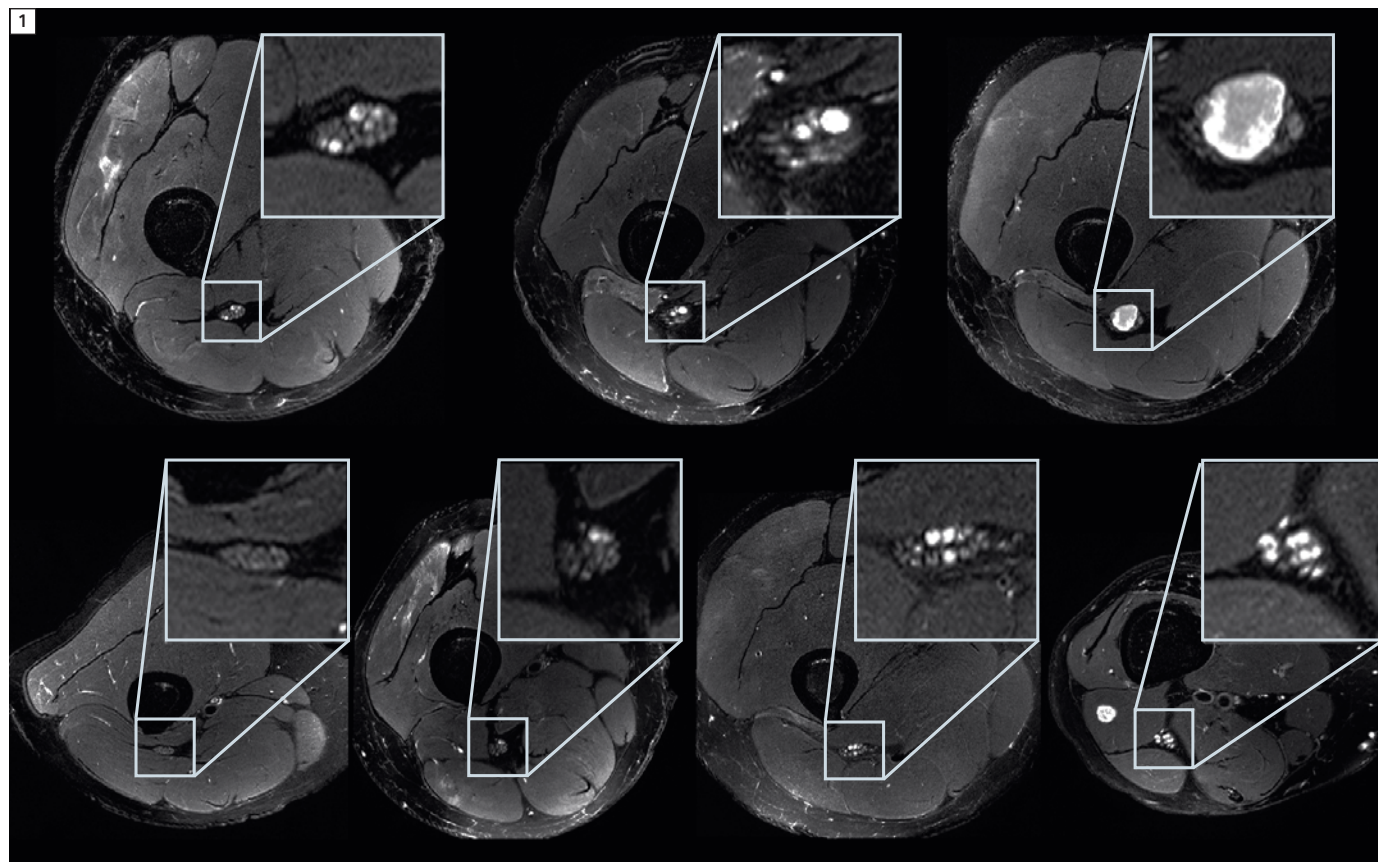
1 T2-weighted sequence with fat saturation at high resolution allows for imaging of peripheral nerves at the fascicular level. The sciatic nerve is shown here in hereditary NF2 polyneuropathy with various lesions ranging in size from pretumorous microlesions affecting only individual fascicles with no significant caliber change (lower row) to severe caliber thickening and enlargement of the entire nerve cross-section as in true, full-blown schwannomas (upper row, right panel). *Modified from Baumer P. et al. Accumulation of non-compressive fascicular lesions underlies NF2 polyneuropathy. J Neurol. 2012, with permission.*

eral nervous system are, as in many diseases of the CNS, arguably among the most important pieces of diagnostic information.

One typical example for the use of MRN is the differentiation between spinal nerve root compression (radiculopathy), plexus affection and peripheral nerve lesion (peripheral neuropathy). Another frequent and important situation is the differentiation of a focal mononeuropathy, which is potentially surgically amenable, from neuropathies with involvement of more than one nerve. These oligo- or polyneuropathies almost exclusively exhibit a disseminated lesion pattern stemming from an inflammatory,

immune-mediated, metabolic or hereditary origin, so that nerve surgery is not a primary therapeutic option.

In traumatic nerve injuries, exact lesion localization is the central diagnostic step in pre-surgical work-up. The assessment of nerve continuity and the identification of potential scar tissue within and around the nerve yield essential diagnostic information. In cases of true neuroma with discontinuity of the nerve, early indication for reconstructive nerve surgery by MRN can improve outcome. However, in instances where MRN shows a neuroma in continuity, surgery may become unnecessary since spontaneous recovery may occur under clinical monitoring.

II) How I do it

a) MRN protocol

A magnetic field strength of 3 Tesla is advisable to achieve high-resolution images at the fascicular level of peripheral nerves. We perform clinical examinations on a Siemens MAGNETOM Verio 3 Tesla MR System (Siemens Healthcare, Erlangen, Germany) which allows comfortable positioning due to its wide bore diameter. The MRN protocol varies depending on the body region of interest and the clinical-diagnostic question. In the vast majority of patients, T2-weighted fat-saturated sequences are acquired, which show high contrast of nerve lesions to
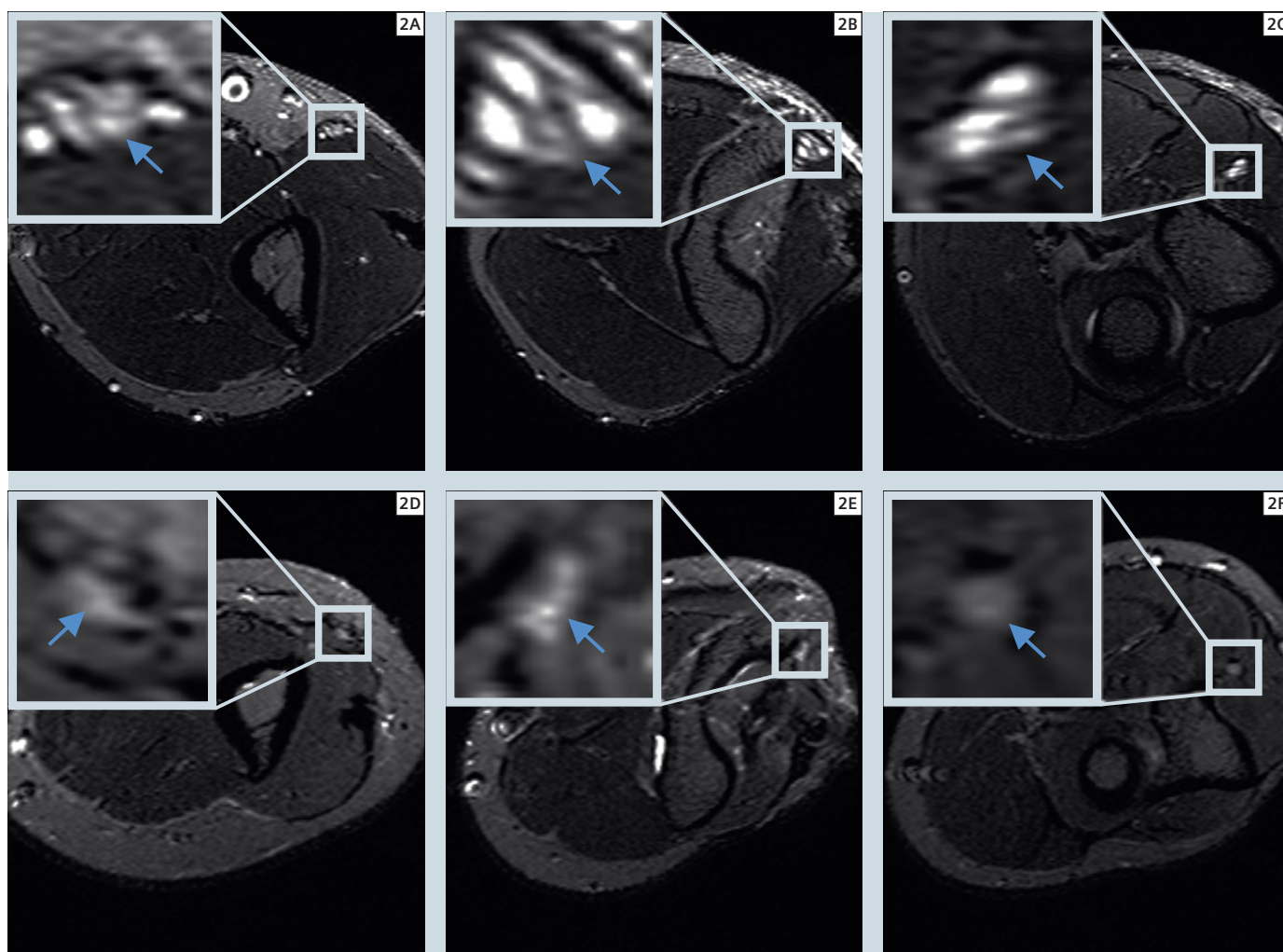
2 Typical findings in cubital tunnel syndrome, a common entrapment neuropathy. The upper row depicts a typical compressive focal ulnar nerve lesion at the elbow from proximal **(2A)** to distal **(2C)**. Nerve T2w signal and caliber are severely increased compared with healthy control (lower row). *Modified from Baumer P. et al. Ulnar neuropathy at the elbow: MR neurography-nerve T2 signal increase and caliber. Radiology. 2011;260(1):199-206, with permission.*
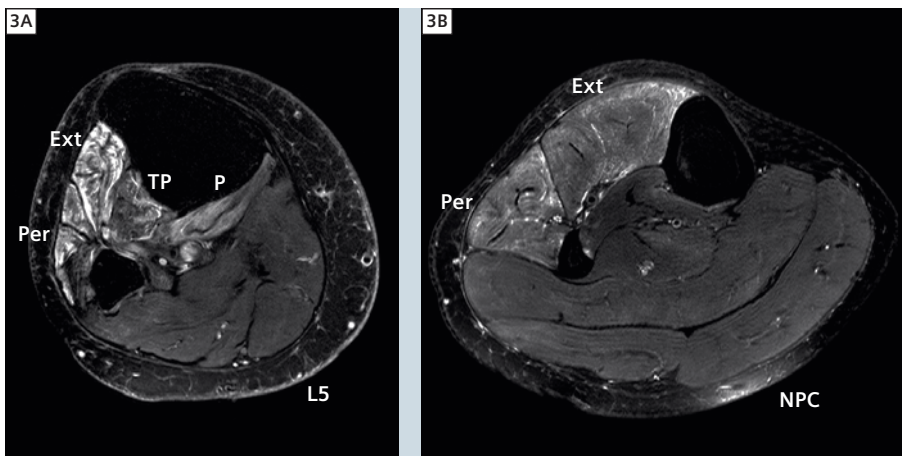
3 Inferring the site of nerve lesion from the comprehensive evaluation of muscle denervation patterns. **(3A)** The denervation pattern in a patient with an L5 lesion additionally includes the posterior tibial muscle and the popliteal muscle. **(3B)** Patient with a lesion of the common peroneal nerve (NPC). The denervation is confined to the extensor compartment (here shown the anterior tibial muscle and extensor digitorum muscle) and the peroneal compartment (long and short peroneal muscle). Both compartments are known to harbor exactly the target muscles of the common peroneal nerve.
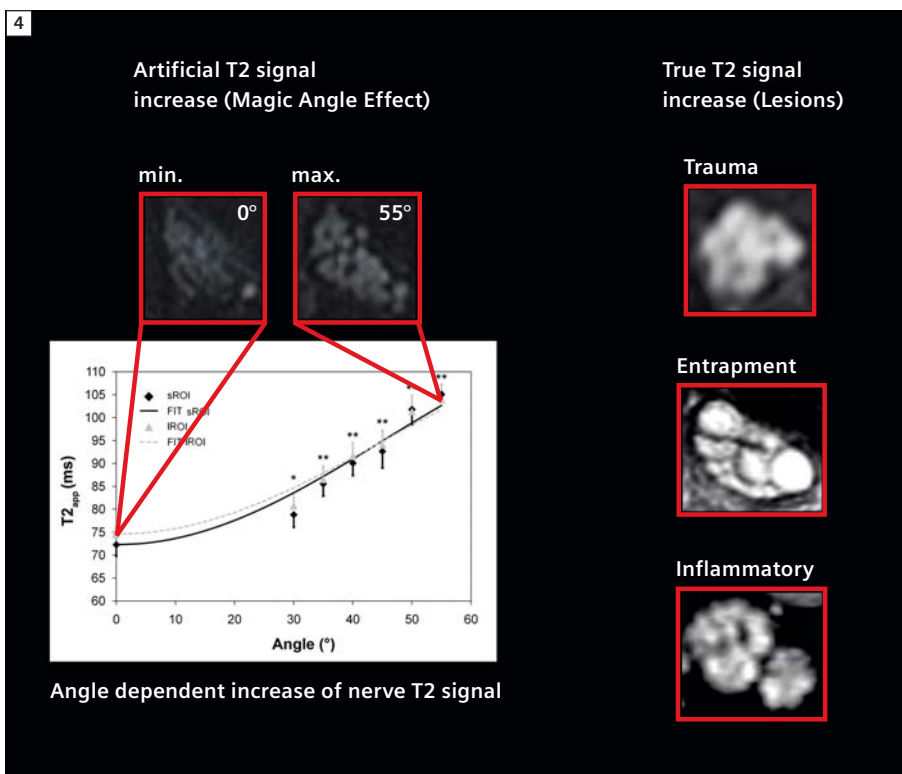

4 The magic angle effect occurs in tissue which is densely composed of collagen, such as in tendons, but also peripheral nerve. On the left the increase in T2 relaxation time can be seen as a function of angular deviation of nerve from the main static magnetic field (B_0). The first maximum of this cosine type function is reached at 55°. The T2 signal increase is visually apparent (zoomed inserts above graph) at the maximum magic angle position of 55° in comparison with the neutral position (0°). However, true nerve lesions in neuropathies of various origins can usually be discriminated easily by the much stronger T2 signal increase (right column, traumatic, compressive and inflammatory true nerve lesions). *Modified from Kaestel et al. AJNR Am J Neuroradiol. 2011 May;32(5):821-7, with permission.*

surrounding tissue (Fig. 1). This may be complemented by T1-weighted sequences, with and without contrast administration, and T1-VIBE or TrueFISP for 3D reconstruction. T2-weighted SPACE STIR sequences at isotropic voxel size allow for imaging at submillimeter resolution of brachial and lumbosacral plexus structures. CISS may be added for imaging of intradural filaments in cases of trauma. Choosing appropriate radio-frequency coils is crucial for image quality and diagnostic performance. For extremities, we use an 8-channel knee coil (Siemens Healthcare, Erlangen, Germany) for most regions. For brachial plexus structures, we additionally acquire high-resolution sequences using dedicated surface coils (multichannel phased-array 2 element coil, NORAS GmbH, Höchberg, Germany).

The applicability of diffusion tensor imaging (DTI) by echo-planar-imaging (EPI) has been investigated for many years [3]. It is currently not used in routine clinical examinations and its diagnostic accuracy has so far only been studied for carpal tunnel syndrome [4].

Various technical issues may limit the clinical significance of application of EPI DTI in the near future, most importantly its structural resolution, which is significantly inferior to T2-weighted sequences and constrains its use to large peripheral nerves of the extremities. Segmented EPI could help to overcome these limitations. Extent of coverage of an MRN examination is decided on a case-by-case basis. In the setting of focal nerve damage, the examination can be targeted to one region by different sequences. Occasionally, larger coverage of an entire extrem-
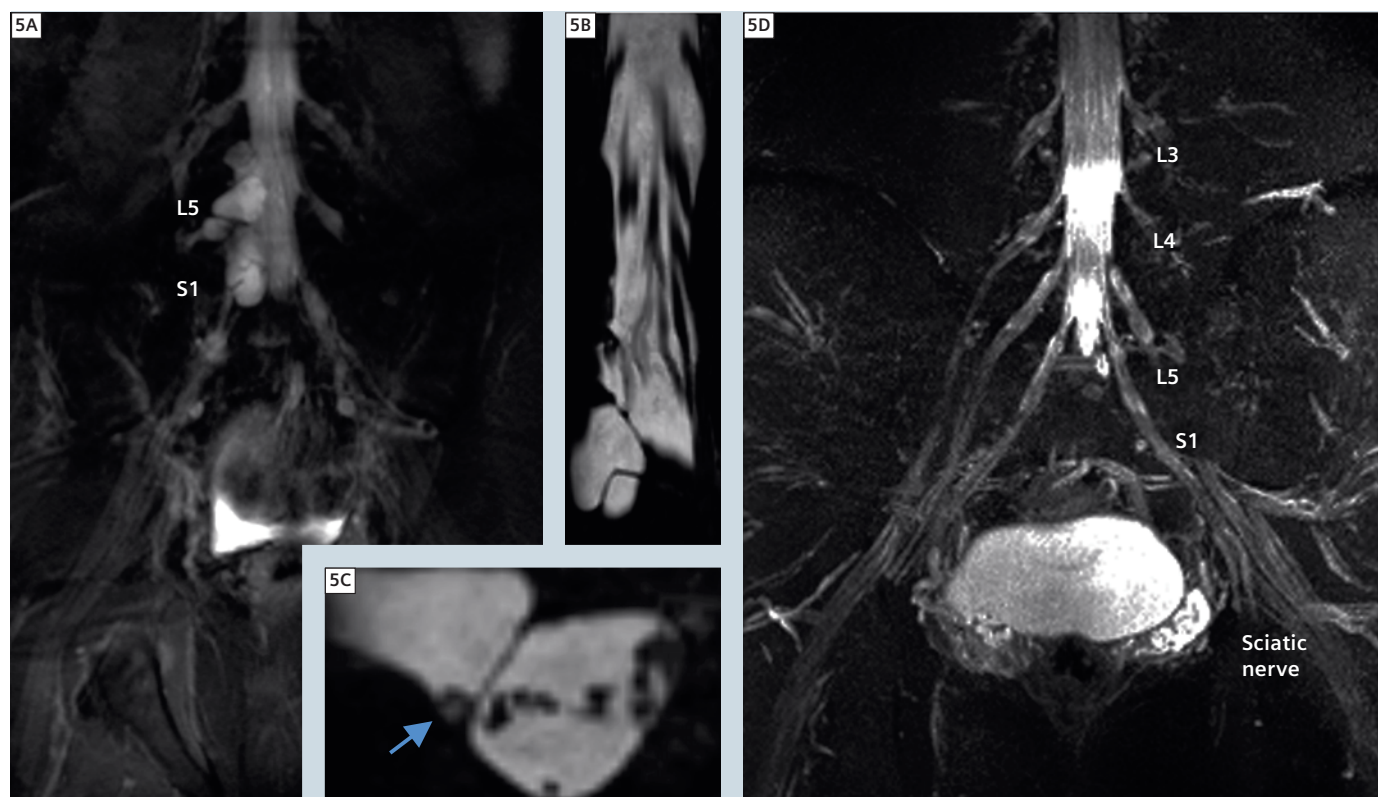
5 Traumatic lumbosacral plexus injury. **(5A)** Coronal SPACE STIR gives an overview of lumbosacral plexus and proximal sciatic nerve. Pseudo-meningoceles of L4 – S 2/3 indicate root avulsions on the right side. **(5B)** Additional CISS of the lumbosacral spinal canal in coronal reconstruction confirms roots avulsions of L5 – S2. **(5C)** Axial reconstruction of CISS. Dorsal portions of the right L4 root appear intact at least in their intraspinal course. **(5D)** Coronal SPACE STIR maximum intensity projection (MIP) of a normal lumbosacral plexus including the proximal sciatic nerve.

ity including the plexus and at the same time high resolution may be useful. One such example is the hereditary polyneuropathy in neurofibromatosis type II [5] where a large number of microlesions may lead to motor and sensory loss but a single, surgically removable macrolesion must be ruled out. Also, large coverage MRN is able to characterize the spatial pattern of polyneuropathies such as diabetic polyneuropathy [6].

b) Diagnostic criteria
Nerve T2 signal is a highly sensitive and specific diagnostic sign for the presence of neuropathy [7]. Increased T2 signal as a parameter of high pathomorphogical contrast is readily assessed by qualitative visual evaluation. Nerve caliber is a second important diagnostic sign and, when clearly increased, usually indicates the presence of a more severe neuropathy. Looking beyond the nerves, the denervation pattern of muscles adds crucial infor-

mation [8]. It can help establish the site of a nerve lesion, as in L5 radiculopathy compared to common peroneal neuropathy (Fig. 3).

Contrast enhancement of peripheral nerves is observed in cases of peripheral nerve sheath tumors such as neurofibromas, schwannomas and perineuriomas. Whether contrast uptake can discriminate between different tumor entities and dignities has not been formally investigated. In cases of potential nerve trauma, nerve continuity is a straightforward but essential criterion when a 'true' neuroma has to be discriminated from a neuroma-in-continuity.

c) Pitfalls
The magic angle effect causes an increase in T2 of fibrous tissue densely packed with collagen which results in artificially bright signal in T2w images. The magic angle effect depends on the angular orientation of the main longitudinal axis of the inves-

tigated structure (e.g. a tendon or peripheral nerve) relative to the field direction of the main static magnetic field (B_0) and reaches its maximum at 55°. It is related to the interaction of collage bound protons and can also be observed in the peripheral nervous system [9, 10]. Below an angle of < 30° the artifact becomes negligible so that correct positioning of limbs in an MRN examination can usually avoid its occurrence [10]. There are two regions where an oblique anatomical orientation of nerves cannot be avoided in the scanner: the supraclavicular brachial plexus and the proximal common peroneal nerve. Hence, in these regions, the magic angle must always be considered in image interpretation.

A second pitfall in MRN image interpretation is the presence of small epineural (outside the epineurium as the outer nerve sheath), epineurial (inside the epineurium), and intraneural vessels (within the interfascicular space). Small veins
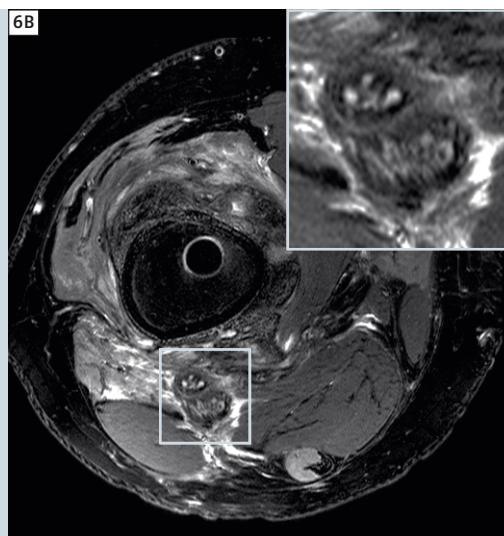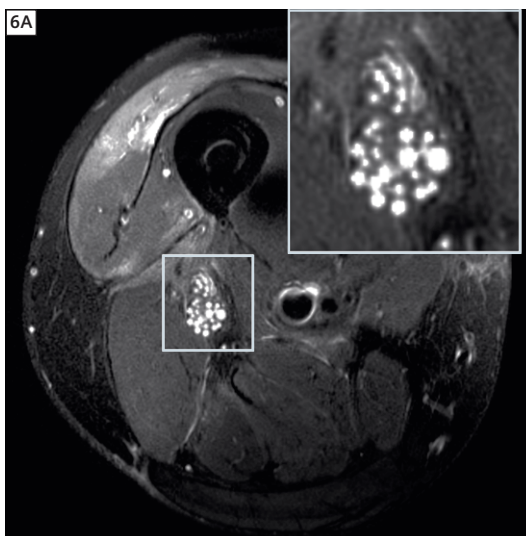
6 Neuroma of sciatic nerve. (**6A**) Patient with severe trauma and complete disruption of sciatic nerve continuity. Proximal neuroma stump with severely swollen, T2w hyperintense fascicles. (**6B**) Distal neuroma stump with pronounced swelling of epineural tissue.
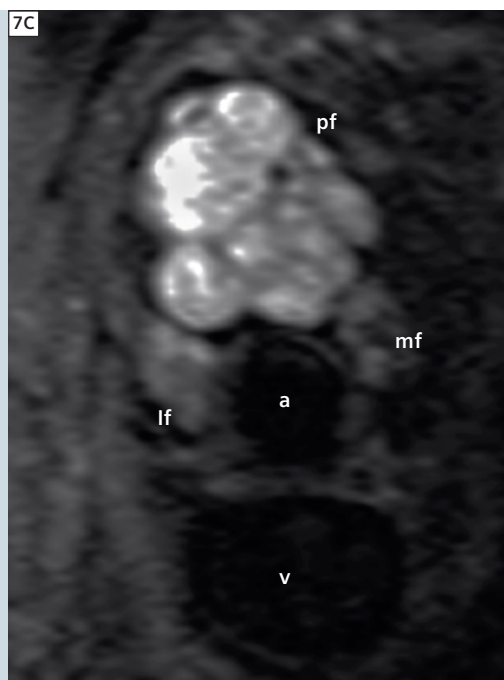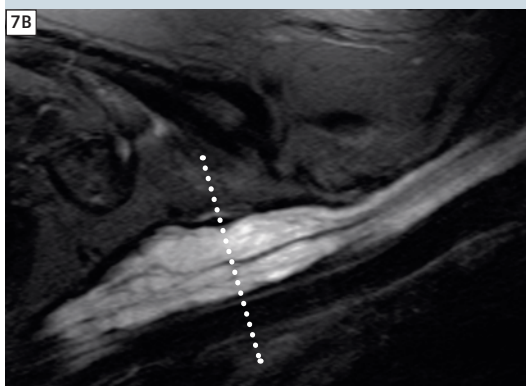
7 Confirmation and localization of inflammatory neuropathy. (**7A**) Composed coronal SPACE STIR sequence in maximum intensity projection (MIP) provides an overview of the brachial plexus on both sides. Spinal nerves are well delineated and can be differentiated from each other. Note the severe distal plexus enlargement on the right side. (**7B**) Additional coronal T2-weighted TIRM gives a high resolution image of the more distal plexus portions of truncs and cords. (**7C**) Sagittal-oblique TIRM through the cords allows precise localization of lesions. In this case the posterior cord is severely enlarged with minor involvement of the lateral and medial cord.

and nerve lesions can have a similar T2 signal intensity. In most cases, small veins are readily discriminated from nerve lesions due to their winded course, strong and relatively homogeneous T2w hyperintense signal, and their eventual anatomical entry or exit into the nerve via its epineurial surface. When in doubt, one proposed method to discriminate the two is to acquire an SSFP sequence [11, 12]. Another approach is to acquire T1-weighted images with fat saturation after administration of contrast media since nerve lesions do not enhance as strongly as vessels.

III) Useful applications of MR Neurography

a) Focal compressive and traumatic lesions

Typical frequent referrals for an MRN exam include suspected compressive neuropathies such as ulnar neuropathy at the elbow or at the wrist. MRN has a high diagnostic accuracy in confirming or excluding these [7, 13]. Main diagnostic criteria are T2 signal and caliber increase. Other frequent focal neuropathies are traumatic nerve injuries. For patients in whom the region of the nerve lesion is known, MRN is most useful in determin-

ing whether continuity of the nerve is intact as well as the precise localization of neuroma (Fig. 6).

In other cases, the exact lesion localization and pattern can only be established by MRI. This is often the case in plexus injuries where electrodiagnostics are limited (Fig. 5). Precise determination of lesion pattern and lesion localization by MRN allows targeted surgery.

Table 1: Exemplary MRN sequences.

Sequence	TR	TE	TI	Slice thickness	Pixel spacing	FOV	Matrix	Slices	Averages	Coil
SPACE STIR coronal	3800	267	180	0.8	0.781 x 0.781	250	320/314	72	2	neck (Siemens)
T2 SPAIR sagittal-oblique	5530	45		3.0	0.469 x 0.469	150	320/198	51	4	dedicated surface coil (NORAS GmbH)
T2 fat-saturated axial	7020	52		3.0	0.300 x 0.300	130	512/358	45	3	knee 8-channel phased-array (Siemens)

b) Disseminated inflammatory lesions

Known or suspected disseminated nerve lesions require an examination tailored to the needs of the individual patient. In suspected inflammatory neuropathy, the precise spatial pattern of involvement of nerves is diagnostically important for classification and treatment. MRN is an excellent method to investigate this even in the most complex nerve structures like the brachial plexus. Figure 7 illustrates the precision of the method.

c) Distal symmetric polyneuropathies such as diabetes mellitus associated PNP

In addition to its manifold clinical applications, MRN contains immense potential for understanding and monitoring the evolution of peripheral nerve disease. In diabetic neuropathy for example, as a typical symmetric polyneuropathy with mainly distal symptoms, the MRN findings of a largely proximal lesion pattern are enhancing our understanding of the pathophysiology of the disease. MRN could for the first time document proximal nerve lesions *in-vivo* [6]. These findings promise a useful research purpose for MRN: to monitor the evolution of nerve lesions in diffuse polyneuropathies and better understand if proximal nerve lesions cumulate to cause distal symptoms, an intriguing pathomechanisms which so far has not been proven by any other clinical-diagnostic or scientific method of investigating nerve pathology.

References

1 Bendszus M, Stoll G. Technology insight: visualizing peripheral nerve injury using MRI. Nat Clin Pract Neurol. 2005;1(1):45-53.

2 Filler AG, Howe FA, Hayes CE, et al. Magnetic resonance neurography. Lancet. 1993;341(8846):659-61.

3 Hiltunen J, Suortti T, Arvela S, Seppa M, Joensuu R, Hari R. Diffusion tensor imaging and tractography of distal peripheral nerves at 3 T. Clin Neurophysiol. 2005;116(10):2315-23.

4 Hiltunen J, Kirveskari E, Numminen J, Lindfors N, Goransson H, Hari R. Pre- and post-operative diffusion tensor imaging of the median nerve in carpal tunnel syndrome. Eur Radiol. 2012;22(6):1310-9.

5 Baumer P, Mautner VF, Baumer T, et al. Accumulation of non-compressive fascicular lesions underlies NF2 polyneuropathy. J Neurol. 2012.

6 Pham M, Oikonomou D, Baumer P, et al. Proximal neuropathic lesions in distal symmetric diabetic polyneuropathy: findings of high-resolution magnetic resonance neurography. Diabetes Care. 2011;34(3):721-3.

7 Baumer P, Dombert T, Staub F, et al. Ulnar Neuro-pathy at the Elbow: MR Neurography-Nerve T2 Signal Increase and Caliber. Radiology. 2011;260(1):199-206.

8 Bendszus M, Wessig C, Reiners K, Bartsch AJ, Solymosi L, Koltzenberg M. MR imaging in the differential diagnosis of neurogenic foot drop. AJNR Am J Neuroradiol. 2003;24(7):1283-9.

9 Bydder M, Rahal A, Fullerton GD, Bydder GM. The magic angle effect: a source of artifact, determinant of image contrast, and technique for imaging. J Magn Reson Imaging. 2007;25(2):290-300.

10 Kastel T, Heiland S, Baumer P, Bartsch AJ, Bendszus M, Pham M. Magic Angle Effect: A Relevant Artifact in MR Neurography at 3T? AJNR Am J Neuroradiol. 2011;32(5):821-7.

11 Zhang ZW, Song LJ, Meng QF, et al. High-resolution diffusion-weighted MR imaging of the human lumbosacral plexus and its branches based on a steady-state free precession imaging technique at 3T. AJNR Am J Neuroradiol. 2008;29(6):1092-4.

12 Chhabra A, Soldatos T, Subhawong TK, et al. The application of three-dimensional diffusion-weighted PSIF technique in peripheral nerve imaging of the distal extremities. J Magn Reson Imaging. 2011;34(4):962-7.

13 Kollmer J, Bäumer P, Milford D, et al. T2 signal of ulnar nerve branches at the wrist in guyon's canal syndrome. PLoS One. Accepted.

Contact
Philipp Bäumer, M.D., M.Sc.
Department of Neuroradiology
Heidelberg University Hospital
Im Neuenheimer Feld 400
69120 Heidelberg
Germany
Phone: +49-6221-56-39670
Fax: +49-6221-56-4673
philipp.baeumer@med.uni-heidelberg.de

High-Resolution DWI in Brain and Spinal Cord with *syngo* RESOLVE[1]

Julien Cohen-Adad

Department of Electrical Engineering, Ecole Polytechnique de Montreal, QC, Canada
A. A. Martinos Center for Biomedical Imaging, Massachusetts General Hospital, Harvard Medical School, Charlestown, MA, USA

Abstract

In this paper we present some applications of the *syngo* RESOLVE[1] sequence that enable high-resolution diffusion-weighted imaging. The sequence is based on a readout-segmented EPI strategy, allowing susceptibility distortions and T2* blurring to be minimized. The RESOLVE[1] sequence can be combined with other acquisition strategies such as reduced field-of-view (FOV) and parallel imaging, to provide state-of-the-art tractography of the full brain and cervical spinal cord. The RESOLVE[1] sequence could be of particular interest for ultra high field systems where artifacts due to susceptibility and reduced T2 values are more severe. At all field strengths, the sequence promises to be useful in a number of clinical applications to characterize the diffusion properties of pathology with high resolution and a low level of image artifact.

1. Introduction

### 1.1. Diffusion-weighted imaging

Diffusion-weighted MRI makes it possible to map white matter architecture in the central nervous system based on the measurement of water diffusion [11]. The technique works by using MRI sequences that are sensitized to the microscopic motion of water molecules, which are in constant motion in biological tissues (Brownian motion). Using the well-known pulse sequence introduced by Stejskal and Tanner in 1965 [29], it is possible to quantify the extent of water displacement in a given direction. This sequence consists of magnetic field gradient pulses (diffusion-encoding gradients) that are applied before and after a 180° radiofrequency (RF) refocusing pulse. The first gradient pulse dephases the precessing nuclear spins that generate the signal in MRI. In the theoretical case of static molecules, the second gradient pulse completely rephases the spins and there is no attenuation due to the application of the gradients. However, if water molecules move during the application of this pair of gradients, spins are dephased and signal decreases as a function of the magnitude of the displacement, leading to a so-called diffusion-weighted signal. The magnitude by which the signal is weighted by diffusion is dictated by the so-called *b-value*, which depends on the length and amplitude of the applied diffusion-encoding gradients, as well as the duration between the first and the second gradient pulse (also called diffusion time). By applying diffusion gradients in various directions (e.g., 20 directions equally sampled on a sphere), it is possible to estimate the rate and direction of water diffusion. For example in pure water, molecules diffuse equally in all directions, hence the diffusion is described as *isotropic*. Conversely, in mesenchymal structures such as the white matter or muscles, water diffuses preferentially along the direction of the fiber. In such a case, the diffusion is *anisotropic* [3].
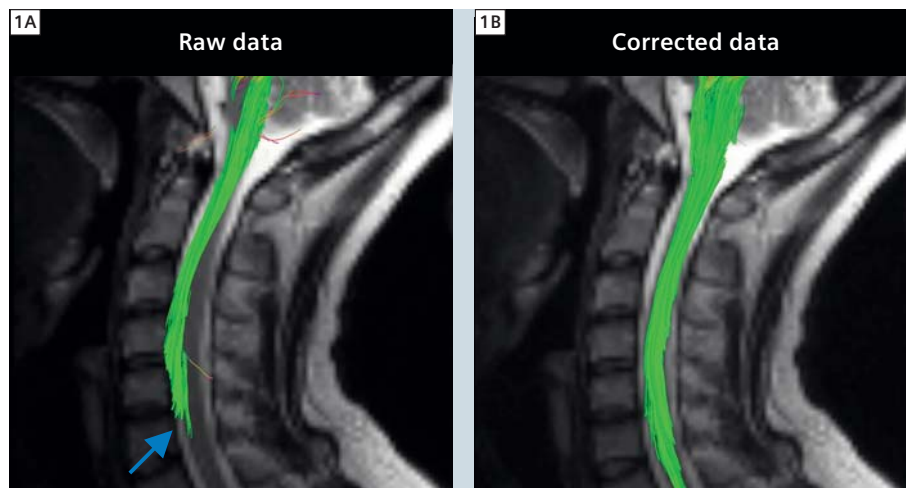
1 Tractography in a healthy subject, overlaid on a distortion-free anatomical image (fast spin echo). **(1A)** shows tractography performed on the raw data (i.e., without correction). **(1B)** shows tractography performed on the same dataset, after distortion correction using the reversed-gradient technique [13]. A false apparent interruption of the tracts is observed on the data hampered by susceptibility distortions. Acquisition was performed using the standard EPI sequence with the following parameters: sagittal orientation, TR/TE = 4000/86 ms, 1.8 mm isotropic, R = 2 acceleration. Tractography was seeded from a slice located at C1 vertebral level.

[1] The software is pending 510(k) clearance, and is not yet commercially available in the United States and in other countries.
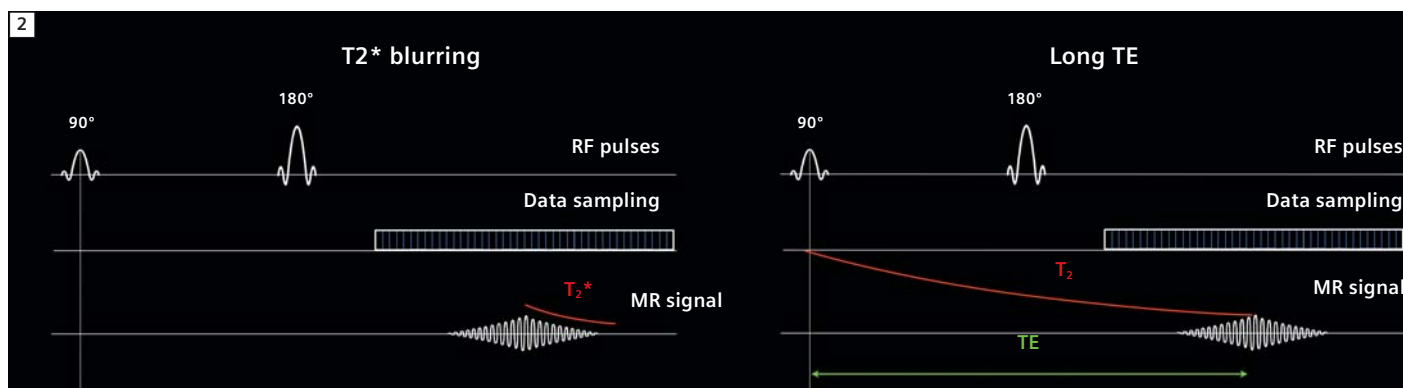
2 The left panel illustrates the origin of the T2* blurring effect, which is caused by T2* dephasing during *k*-space (raw data) sampling. The right panel illustrates the consequence of a long TE due to the combination of the diffusion-encoding gradients and the extended data sampling interval, resulting in low SNR data.

1.2. DTI and tractography

After acquiring a set of diffusion-weighted data, it is possible to compute a parametric model representing the main diffusion direction at each voxel [2]. This type of model is described by a tensor and is usually represented graphically as a 3D ellipsoid. This technique is known as Diffusion Tensor Imaging (DTI) and makes it possible to derive metrics such as fractional anisotropy (FA), mean diffusivity and axial and radial diffusivities. These metrics are relevant as they have been shown to correlate with demyelination and axonal degeneration [28] and can therefore be used to obtain markers of demyelination in multiple sclerosis [26], spinal cord injury [7] or amyotrophic lateral sclerosis [8].

Having modeled the diffusion tensor, it is possible to reconstruct global axonal pathways by linking every voxel with a similar eigenvector (principal axis of the diffusion tensor) to its neighbors. This procedure is called fiber tracking or tractography [18]. It should be mentioned however that the reconstructed fiber bundles do not represent *real* axonal tracts but rather represent the path where water diffuses preferentially. It is therefore an indirect measure of axon orientation. Hence, tractography results should be handled with care since they may not represent the real pathway of axons [14]. For instance, false negatives could be induced by the presence of crossing fibers, which would artificially

decrease the FA and stop the tracking procedure. Inversely, false positives could be induced by fibrous structures such as scar tissue, in which water diffusion also has anisotropic properties [27]. In such cases, fiber tracking can become fiber *tricking*.

To illustrate the need for caution, Figure 1 shows an example of tractography performed in a healthy subject, before and after correction for susceptibility artifacts, which can induce strong image distortions in the phase-encoding direction (antero-posterior in this example). On the 'raw data' (1A), a false apparent interruption of the tracts is clearly observed, and can be misinterpreted as an interruption of the white matter tracts. However, this apparent interruption is simply due to susceptibility distortions, as can be seen on the 'corrected data' (1B). This result suggests two things: *(I)* a careful assessment of the image data is essential before further processing is applied and *(II)* susceptibility-induced distortions should be minimized by an appropriate choice of data acquisition technique. This might ultimately reduce the need for quality assessment, which is not often possible in clinical routine. This brings us to the next section on how to reduce susceptibility artifact during the acquisition.

1.3. Artifacts in diffusion-weighted imaging

In this section we will mostly focus on susceptibility artifacts and T2* blurring. Other artifacts exist in diffusion-weighted imaging [15], but are not in the scope of the presence article. Single-shot echo planar imaging (ss-EPI) is an ultra-fast imaging sequence that makes it possible to acquire a full slice within a single repetition time (TR) [16]. To achieve this, spatial encoding gradients are played out rapidly along two gradient axes (e.g. X and Y) in order to sample all raw data (or *k*-space) points in a 'single shot' after an RF excitation pulse. By applying the EPI readout directly after the excitation pulse, a gradient echo image can be generated. Alternatively, an RF refocusing pulse can be inserted between the excitation and EPI readout to produce a spin echo image, which has reduced susceptibility-induced signal loss, but has the same sensitivity to susceptibility-based distortions. An oscillating readout gradient is applied along one axis (e.g. X), consisting of a series of gradient pulses with alternating polarity and each of these readout gradient pulses is used to sample a single line of *k*-space. A short phase-encoding gradient or 'blip' is applied along an orthogonal gradient axis (e.g. Y), so that each readout gradient corresponds to a different line of *k*-space in the Y direction. While acquisition of a full line a *k*-space in the read-

out direction is obtained rapidly (in about 1 ms), the acquisition of k-space data along the phase-encoding direction takes much more time. For example, for a 128 × 128 matrix, acquisition of the full k-space can take more than 100 ms. During that time, spins experience dephasing due to local B_0-inhomogeneities. These undesirable inhomogeneities are typically induced at interfaces between structures with different susceptibility properties, such as air/tissue or bone/muscle. As a result, phase errors accumulate in the phase-encoding direction, causing geometric distortions in the reconstructed image in that direction. EPI sequences are fast and particularly appropriate for diffusion-weighted experiments [31] where multiple datasets need to be acquired in a clinically acceptable time with low sensitivity to motion-induced phase error [17]. However single-shot EPI also has the disadvantage that it is particularly sensitive to susceptibility-related geometric distortions. Reduction of susceptibility artifacts can be achieved by sampling the k-space faster, which decreases the accumulation of the phase errors. Faster acquisition can be achieved by reducing the echo spacing, which is defined as the total time between the application of two phase-encode blips. Echo spacing can be reduced by (I) increasing the readout bandwidth, (II) reducing the number of phase lines by reducing the FOV (because the sampling density in k-space defines the FOV in the image domain) and (III) combining several sub-sampled k-space acquisitions (multi-shot). In addition to susceptibility artifacts, T2* blurring can be induced due to the relatively long sampling of k-space, during which T2* relaxation occur (Figure 2, left). This effect is more pronounced in regions with large B_0 inhomogeneities. Another undesirable effect of the long sampling is that it will impose a relatively long echo time (TE) (Figure 2, right). As a result, the recorded signal amplitude will be small due to the relatively short transverse relaxation (T2) in white matter (about 70 ms at 3T). This effect is critical since SNR is proportional to exp(-TE/T2), therefore even
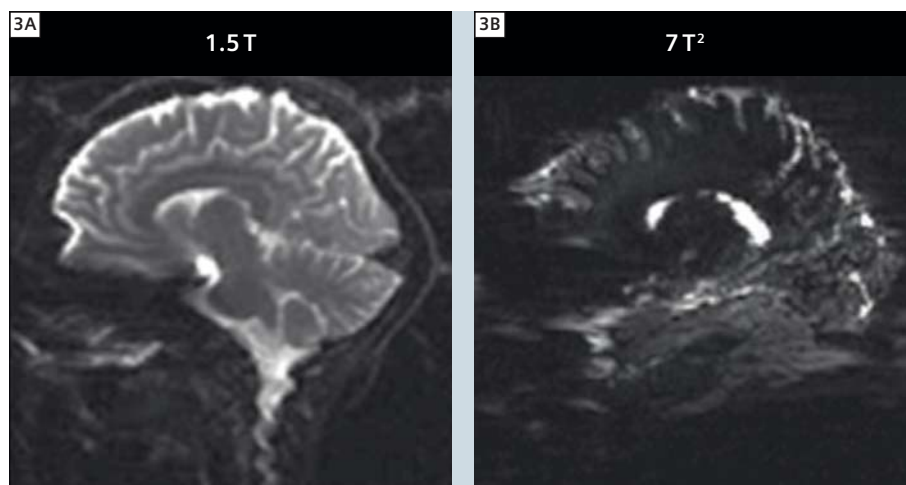
3 Comparison of single-shot EPI at 1.5T **(3A)** and 7T[2] **(3B)**.

4 Benefits of faster sampling for: (I) reducing susceptibility distortions (less accumulation of phase errors), (II) reducing T2* blurring (faster sampling) and (III) enabling shorter TE (due to the faster sampling of k-space, which in turn brings the center of the readout window closer to the 180° pulse).

a small increase of TE (several ms) can substantially reduce the signal-to-noise ratio (SNR).

All these limitations become even more problematic at higher field, where T2 is reduced (about 50 ms at 7T) and B_0 homogeneity is more difficult to achieve, resulting in a greater level of susceptibility artifact. Figure 3 shows an example of the high-field degradation in image quality when using the standard single-shot EPI technique at 1.5T and 7T[2].

To summarize, the main issues encountered with diffusion-weighting EPI are:

■ **Susceptibility artifacts**, which are caused by an accumulation of phase error during the readout, leading to image distortions.

■ **T2* blurring**, which is caused by the long data sampling interval during the readout, leading to a broadening of the point spread function and a blurring of the reconstructed image.

■ **Long TE**, which is imposed by a combination of the diffusion-encoding gradients and the long data sampling interval and results in low SNR.

These three arguments provide motivation for a reduction in the sampling time, which will address all these issues, as illustrated in Figure 4.

[2]The 7T system is a research system only. It cannot be used outside of a research study.

2. Multi-shot techniques and *syngo* RESOLVE[1]

As described in the previous section, susceptibility artifacts and T2* blurring can be reduced by decreasing the sampling time (or the effective echo spacing). In EPI, this can be done by skipping lines of *k*-space in the phase-encoding direction (also called interleaved EPI). Multi-shot techniques consist of acquiring several sub-sampled images and combining them to reconstruct a full *k*-space data set. An example of a 2-shot interleaved EPI acquisition is illustrated in Figure 5. In this approach, the first image is acquired by only filling even lines of *k*-space, while the second image is acquired by filling the odd lines. Then, both data sets are combined in order to obtain the full *k*-space data that is required for image reconstruction. The key aspect is that each of the sub-sampled data sets is acquired twice as fast as in the single-shot case, which reduces the effective echo spacing by a factor two, and hence also reduces the distortions by a factor of 2. However, one disadvantage of the interleaved EPI approach is that the overall acquisition time is longer than single-shot techniques (because multiple TR intervals are required acquire all data required to form an image). Another disadvantage is that phase errors due to motion (from subject or physiology) can occur between the acquisition of different interleaves, which can lead to severe ghosting artifacts [6].

To overcome the mismatch between different data interleaves, one can acquire navigator echoes that monitor phase errors and correct them before image reconstruction. At their introduction, navigator echoes consisted in single line of *k*-space acquired at the center, which was used to apply a linear phase correction in the readout direction [1, 20]. Later, 2D navigator echoes enabled linear phase correction both in the readout- and in the phase-encoding directions [4]. More recently, non-linear approaches have been introduced [17], which is particularly important for diffusion-weighted imaging of the brain, where cerebrospinal fluid pulsation leads

to non-rigid-body brain motion that results in non-linear phase errors if the motion occurs during the application of the diffusion-encoding gradients. 2D non-linear phase correction is most easily applied when each shot in the multi-shot data acquisition samples a contiguous set of data points from a sub-region of *k*-space. In this case, the Nyquist sampling condition is fulfilled and the phase correction can be applied as a complex multiplication in image space. The interleaved EPI sampling scheme does not fulfill this local Nyquist sampling condition and results in aliased signal contributions that complicate the phase correction procedure.

2.1. Readout-segmented EPI

An alternative to the interleaved approach is to perform readout-segmented EPI [25]. In readout-segmented EPI, *k*-space

is filled with a series of concatenated segments in the readout direction (Figure 6), corresponding to shorter readout gradient pulses and an overall reduction in the length of the EPI readout As with interleaved EPI, the shorter readout time results in a reduction in the level of susceptibility-based distortion.
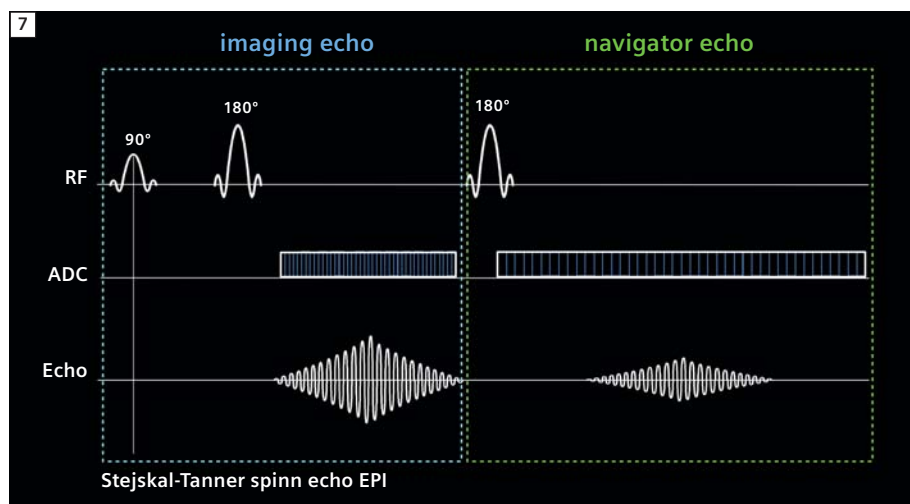
2.2. Diffusion-weighted readout-segmented EPI

One advantage of readout-segmented EPI compared to phase-segmented (or interleaved) EPI is that each segment consists of a Nyquist-sampled region of *k*-space that is well suited to the application of 2D non-linear phase correction, as described above. This property of the readout-segmented EPI sampling scheme was first exploited by Porter et al. [24] who proposed the sequence shown in figure 7 for application to diffusion-
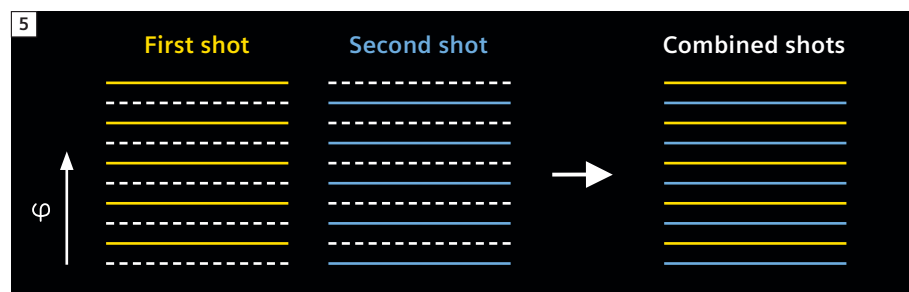
5 Segmented EPI along the phase-encode direction (interleaved EPI). *(I)* Acquire several shots of sub-sampled *k*-space, *(II)* concatenate all shots and *(III)* reconstruct image. Each shot is sub-sampled, resulting in a shorter data sampling interval and reduced distortion.
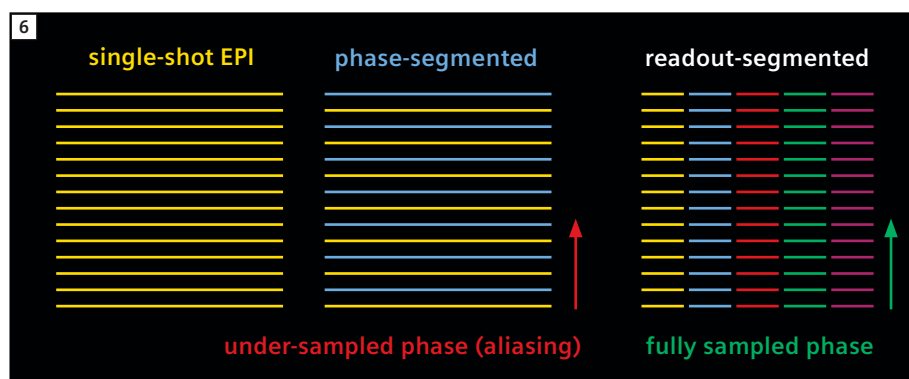
6 Schematic of *k*-space acquired using a conventional single-shot EPI (left), phase-segmented or interleaved EPI (middle) and readout-segmented EPI (right). In the phase-segmented EPI, the data for each shot is sub-sampled in the phase-encoding direction, which induces aliasing and therefore difficulties in correcting for phase-to-phase errors using advanced 2D non-linear techniques. However in readout-segmented EPI, all phase-encode lines are acquired in each shot, therefore there is no aliasing.

7 Simplified pulse diagram of the RESOLVE sequence (gradients are not represented).

weighted imaging. The sequence consists of an imaging echo, which is used to sample the standard readout-segmented EPI data, and a 2D navigator echo, in which a low resolution EPI readout is used to sample the center of *k*-space at each shot. The sequence was subsequently modified to support parallel imaging [22] using GRAPPA [10]. This made it possible to further shorten the readout time with a corresponding additional reduction in the level of susceptibility artifact. The resulting sequence has been given the acronym RESOLVE[1] (Readout Segmentation Of Long Variable Echo-trains).

2.3. Reacquisition technique

In some cases, the level of motion-induced phase error can be too severe for a reliable phase correction due to signal voids in the navigator images. Although physiological gating strategies can be employed to mitigate these effects, they do not address all sources of motion and can significantly increase acquisition time. To avoid the residual artifacts associated with these occasional extreme phase errors, the RESOLVE[1] sequence uses a reacquisition strategy to identify and re-measure corrupt readout segments that cannot be reliably phase corrected. This method is based on an original concept that was proposed for interleaved EPI and 1D navigator echoes [19], but uses

an adapted real-time algorithm, which has been optimized for the combination of 2D navigator data and the readout-segmented EPI sampling scheme [21]. For a comprehensive description of the RESOLVE[1] sequence, including the adaptions for parallel imaging and data reacquisition, the reader is referred to [23].

3. Application of the RESOLVE[1] sequence

To illustrate the benefits of the RESOLVE[1] sequence, Figure 8 shows a comparison between the conventional single-shot EPI (8A) and RESOLVE[1] (8B). Acquisition parameters were:
RESOLVE: Axial slices, TR 3800 ms, TE 80 ms, 4 nex, 12-4 mm thick slices with 0.4 mm gap, 320×256 matrix, b=700 s/mm^2 only in slice direction (S-I), GRAPPA x 2, segment 21, FOV 163 mm, acquisition time 6–7 min (depending on reacquisition).
Single-shot EPI: Axial slices, TR 3800 ms, TE 102 ms, 32 nex, 12–4 mm thick slices with 0.4 mm gap, 192×192 matrix, b=700 s/mm^2 only in slice direction (S-I), GRAPPA x 2, FOV 220 mm, acquisition time 2 min 15 sec.
All scans were performed at 3T using a 32-channel array head coil.
Images represent an axial mean diffusion-weighted image located in the lower brain region, which is well-known for its susceptibility artifacts due to the

sinuses and temporal poles. In the ss-EPI image, strong susceptibility artifacts can be observed as image and signal distortions. For example, the temporal region not only shows image distortion along the phase-encoding direction (antero-posterior), but also shows increase of signal intensity caused by the overlap of distorted voxels (arrow). This spurious signal increase could be falsely interpreted as pathological. Conversely in the RESOLVE[1] image, the same region shows a substantial reduction in this susceptibility artifact. In addition, an overall blurring can be observed on the ss-EPI image, which is caused by the relatively long *k*-space sampling relative to the T2* decay. Reducing the sampling time also reduces this T2* blurring, as can be seen on the RESOLVE[1] image, where the image appears sharper, making it possible to delineated white and gray matter with greater precision.

3.1. 1×1×1 mm³ resolution full brain at 7T

With the RESOLVE[1] sequence it is possible to acquire high-resolution images without the large increase in susceptibility and T2* artifacts that would affect an ss-EPI acquisition. In one study at 7T, the sequence was used to perform full brain diffusion-weighted imaging at $1 \times 1 \times 1$ mm^3 resolution [12]. The study was performed on a whole-body scanner (MAGNETOM 7T[2], Siemens Healthcare, Erlangen, Germany) with a 24-channel RF receive coil (Nova Medical, Wilmington, MA, USA). Acquisition parameters were: 104 axial slices, matrix 220×220, FOV 220 mm, slice thickness 1 mm (no gap), TR 7500 ms, TE 76 ms, 7 readout segments, 30 diffusion-weighting directions at a b-value of 1000 s/mm^2, acquisition time was 78 min. The diffusion-weighted images were filtered with a two-stage hybrid image restoration procedure, corrected for subject motion and registered to a T1-weighted anatomical image (1 mm resolution) of the same participant. For each voxel, multiple fiber orientations were modeled by constrained spherical deconvolution [30] followed by whole-brain fiber-tracking using
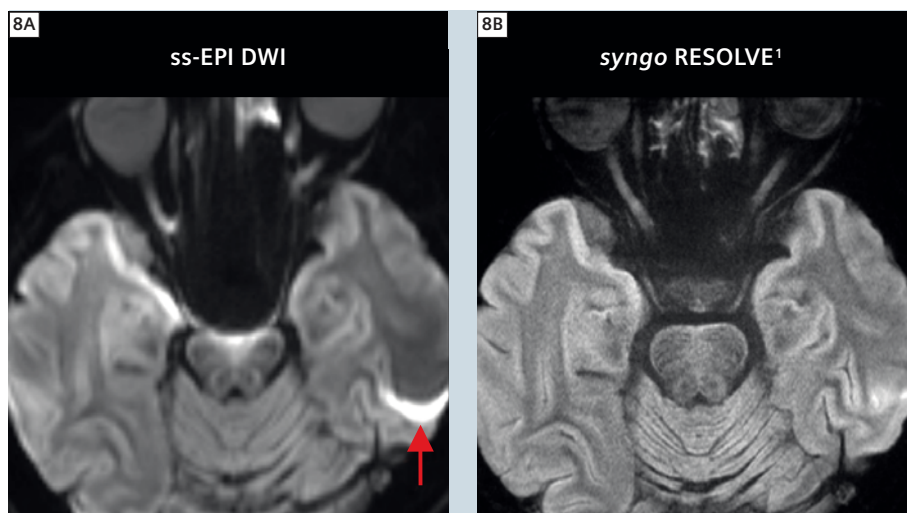
MRtrix (http://www.brain.org.au/software)[3].

Figure 9 shows results of the fiber orientation distribution function (ODF) and tractography centered over the pre-motor cortex. The spatial consistency of the fiber ODF demonstrates the high SNR of the data (Figure 9B). Tractography successfully demonstrated intersection of the corpus callosum (CC, pink), the corona radiata (CR, blue) and the superior longitudinal fasciculus (SLF, green, tracks not shown).

The same data were processed using track-density imaging [5], which makes it possible to reconstruct fiber bundles at 200 μm resolution. Figure 10 shows the results at the three orientations in order to appreciate the 1 mm isotropic resolution. The views are centered over the thalamus. The ultra-high resolution in combination with high SNR and low susceptibility artifacts provide an unprecedented level of detail about the anatomical organization of the thalamus. The ability of the sequence to provide full brain coverage at an isotropic resolution of 1 mm made it possible to reconstruct track density images of the whole brain with no orientation bias.

3.2. Spinal cord DTI at 3T

Another powerful application of the RESOLVE sequence is the spinal cord. Indeed, spinal cord DTI is particularly challenging due to *(I)* the small cross-sectional size of the spinal cord, which requires high spatial resolution, resulting in low SNR at standard imaging times; *(II)* susceptibility artifacts, which are caused by inhomogeneous magnetic field in the spinal region due to the close proximity of tissue with very different magnetic susceptibility (tissue, bone, air, cartilage) and *(III)* physiological-related motion due to respiration, heart beat, cerebrospinal fluid pulsation. The first two arguments (small size and susceptibility artifacts) are particularly well suited for the RESOLVE[1] sequence, as this
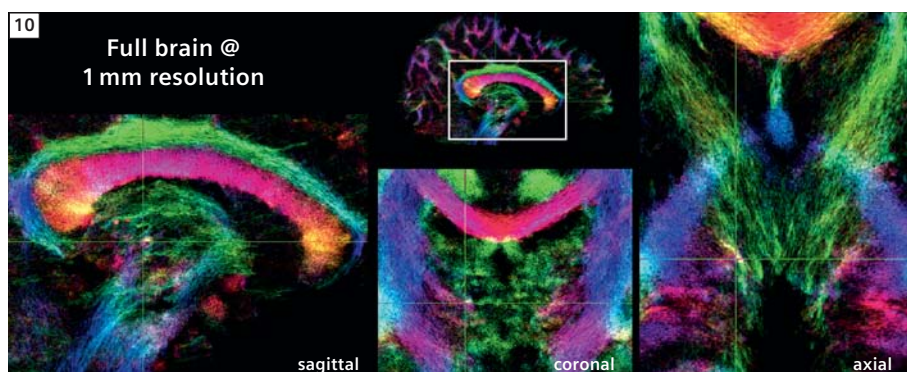
[3]MRtrix is not a Siemens Healthcare product. Siemens bears no responsibility for this product including, but not limited to, its regulatory status. Further information about the software can be found at the website listed.

8 Comparison of standard single-shot EPI sequence **(8A)** and *syngo* RESOLVE[1] **(8B)**. Susceptibility distortions are substantially reduced on the RESOLVE[1] image. For example, the temporal region of the ss-EPI image not only shows image distortion along the phase-encoding direction (antero-posterior), but also shows an increase in signal intensity caused by the overlap of distorted voxels (arrow). Sharper image with RESOLVE[1] also comes from faster sampling, via reduction of T2* blurring. *Images courtesy of Professor Naganawa, Nagoya University School of Medicine, Japan.*
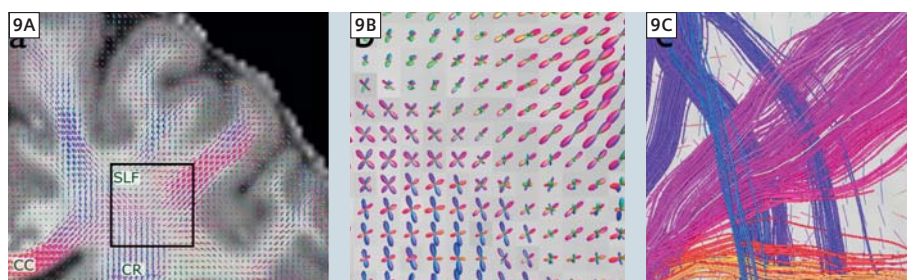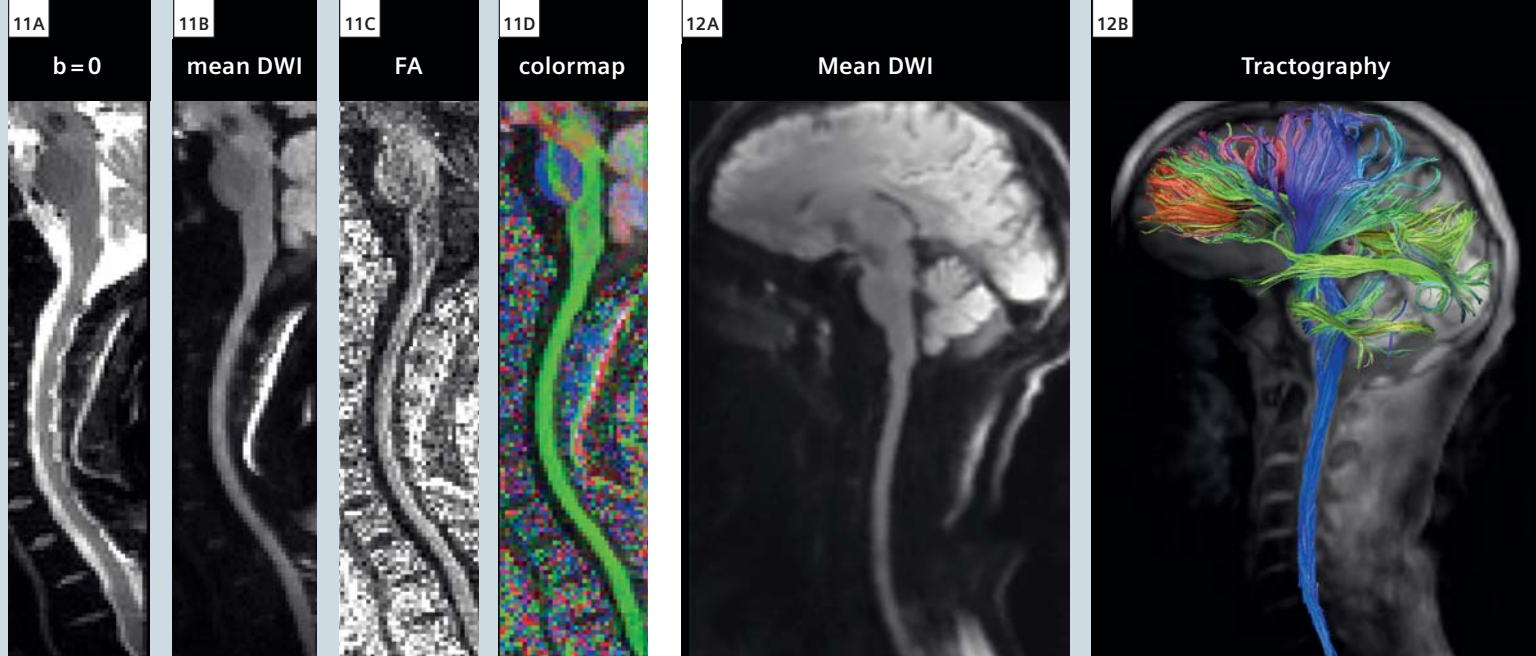

9 High angular resolution diffusion imaging results from 1 mm isotropic resolution. **(9A)** Coronal view centered in the pre-motor region at the intersection between corpus callosum (CC), superior longitudinal fasciculus (SLF) and corona radiate (CR). **(9B)** Orientation distribution functions (ODF) showing crossing of the major pathways. **(9C)** Tractography results showing intersection of the CC (pink) and CR (blue). *Images courtesy of Drs. Robin Heidemann and Alfred Anwander, MPI Leipzig, Germany.*

10 Track density image with 200 μm resolution. Fine details of the structure of the thalamus are visible. *Image courtesy of Drs. Robin Heidemann and Alfred Anwander, MPI Leipzig, Germany.*

11A	11B	11C	11D
b = 0	mean DWI	FA	colormap

11 Human cervical spinal cord. 1.7 mm isotropic, 3 shots, R = 3, TE 74 ms, Cardiac gating, b 800 s/mm², 30 directions in 8 min.

12A	12B
Mean DWI	Tractography

12 Sagittal view of the mean diffusion-weighted images **(12A)** and fiber tractography overlaid on the anatomical image **(12B)**. Almost no distortions are observed, which makes it possible to explore white matter connections from cortical areas down to the spinal cord without spurious interruptions.

sequence provides high SNR and enables reduction of susceptibility distortions. The last challenge (physiological motion) is a typical cause of failure for segmented approaches, however the non-linear 2D phase correction combined with the reacquisition scheme enabled in the RESOLVE[1] sequence ensures low sensitivity to physiological motion.

An example of the RESOLVE[1] in the spinal cord is shown in Figure 11. To further improve image quality, the RESOLVE[1] sequence was used with parallel imaging using the GRAPPA algorithm [10] to further reduce susceptibility artifacts and shorten the TE. To maximize the capabilities of parallel imaging, a dedicated 32-channel head/spine coil was used, which enables up to 4× acceleration [9]. Acquisition parameters were: 1.7 mm isotropic, 3 shots, R = 3 acceleration (iPAT3), TE 74 ms, Cardiac gating, b 800 s/mm², 30 directions, acquisition time 8 min. The sequence only used 3 shots (i.e., 3 segments per k-space), therefore the acquisition was relatively short. Although minor distortions are still visible on the b = 0 image at the level of each intervertebral disk, the spinal cord itself is not affected by these intervertebral distortions as assessed by the mean diffusion-weighted image, the fractional anisotropy (FA) map and the

FA color map. Note the particularly high spatial resolution (1.7 mm isotropic, 4.9 mm³ voxel volume), which is rarely achieved in spinal cord imaging. One particularly difficult acquisition is when one wants to image the full brain and spinal cord. The challenge of B_0-inhomogeneity can be partially overcome when only the spinal cord is imaged by adjusting the shim volume within an elongated box that nicely encompasses the spinal cord. However, when the FOV includes both the brain and spinal cord, it is a difficult for the shimming algorithm to find appropriate fitting coefficients for ensuring B_0-homogeneity both in the brain and spinal cord, due to the complex geometry and the presence of several susceptibility interfaces (sinuses, temporal poles, brainstem, intervertebral disks and lungs). This type of acquisition is therefore particularly well-suited to the RESOLVE[1] sequence.

Images were acquired with the following parameters: 2.2 mm isotropic resolution, matrix 138 × 104, TR ~ 15000 ms (cardiac gating), TE 66 ms, 3 shots, R = 3 acceleration, b 800 s/mm², 30 diffusion-weighting directions, acquisition time 10:45 min. Images were further corrected for residual susceptibility-distortions in the thoracic region (due to the close proximity with the lungs), using the reversed

gradient technique [13]. Tractography was performed using the Diffusion Tool-kit[3] (deterministic FACT algorithm) and displayed with TrackVis[3] (http://www.trackvis.org/). Diffusion-weighted images were then registered to the 1 mm isotropic anatomical image (MPRAGE). Results are shown in Figure 12 and demonstrate reduction of susceptibility artifacts, enabling to explore connections within and between the brain, brainstem and cervical spinal cord.

4. Conclusion

syngo RESOLVE[1] is a useful sequence for acquiring high-quality diffusion-weighted images thanks to the reduction of susceptibility distortion, reduction of T2* blurring, shorter TE (and hence high SNR) and robust correction for motion-induced artifacts. The RESOLVE sequence has shown promising tractography results in the brain and spinal cord, the latter being known for suffering from severe susceptibility artifacts using standard sequences. The RESOLVE sequence can be combined with other acquisition strategies such as reduced field-of-view and parallel imaging. Potential applica-

[3]Diffusion Toolkit and TrackVis are not Siemens Healthcare products. Siemens bears no responsibility for these products including, but not limited to, their regulatory status. Further information about the software can be found at the website listed.

tions in research include the study of white matter architecture in the brain, brainstem and spinal cord, and also the possibility to study fine structure such as the thalamus and the gray nuclei. In clinical application, the reduced level of susceptibility artifact with the RESOLVE[1] sequence can provide better interpretation of abnormalities in white matter pathology. Although acceptable image quality can already be obtained using the conventional single-shot EPI sequence providing shimming is successful, this procedure is strongly user-dependent, subject-dependent and structure-dependent. Because this variability is not acceptable in clinical routine, the RESOLVE[1] sequence has the potential to ensure robust image quality. Moreover, the RESOLVE[1] sequence may be particularly useful in cases where patients have metallic implants, notably in spinal cord injury, where assessing the integrity of spinal pathway would be of tremendous help for patient prognosis.

5. Acknowledgements

[1]The software is pending 510(k) clearance, and is not yet commercially available in the United States and in other countries.
[2]The 7T system is a research system only. It cannot be used outside of a research study.

References

1 Anderson, A.W., Gore, J.C., 1994. Analysis and correction of motion artifacts in diffusion weighted imaging. Magn Reson Med 32, 379-387.

2 Basser, P.J., Mattiello, J., LeBihan, D., 1994. Estimation of the effective self-diffusion tensor from the NMR spin echo. J Magn Reson 103, 247-254.

3 Beaulieu, C., 2002. The basis of anisotropic water diffusion in the nervous system – a technical review. NMR Biomed 15, 435-455.

4 Butts, K., Pauly, J., de Crespigny, A., Moseley, M., 1997. Isotropic diffusion-weighted and spiral-navigated interleaved EPI for routine imaging of acute stroke. Magn Reson Med 38, 741-749.

5 Calamante, F., Tournier, J.-D., Jackson, G.D., Connelly, A., 2010. Track-density imaging (TDI): super-resolution white matter imaging using whole-brain track-density mapping. NeuroImage 53, 1233-1243.

6 Clark, C.A., Barker, G.J., Tofts, P.S., 2000. Improved reduction of motion artifacts in diffusion imaging using navigator echoes and velocity compensation. J Magn Reson 142, 358-363.

7 Cohen-Adad, J., El Mendili, M.-M., Lehéricy, S., Pradat, P.-F., Blancho, S., Rossignol, S., Benali, H., 2011a. Demyelination and degeneration in the injured human spinal cord detected with diffusion and magnetization transfer MRI. NeuroImage 55, 1024-1033.

8 Cohen-Adad, J., El Mendili, M.M., Morizot-Koutlidis, R., Leheircy, S., Meininger, V., Blancho, S., Rossignol, S., Benali, H., Pradat, P.-F., 2012. Involvement of spinal sensory pathway in ALS and specificity of cord atrophy to lower motor neuron degeneration. Amyotroph Lateral Scler doi:10.3109/17482968.2012.701308.

9 Cohen-Adad, J., Mareyam, A., Keil, B., Polimeni, J.R., Wald, L.L., 2011b. 32-channel RF coil optimized for brain and cervical spinal cord at 3 T. Magn Reson Med 66, 1198-1208.

10 Griswold, M.A., Jakob, P.M., Heidemann, R.M., Nittka, M., Jellus, V., Wang, J., Kiefer, B., Haase, A., 2002. Generalized autocalibrating partially parallel acquisitions (GRAPPA). Magn Reson Med 47, 1202-1210.

11 Hagmann, P., Jonasson, L., Maeder, P., Thiran, J.P., Wedeen, V.J., Meuli, R., 2006. Understanding diffusion MR imaging techniques: from scalar diffusion-weighted imaging to diffusion tensor imaging and beyond. Radiographics 26 Suppl 1, S205-223.

12 Heidemann, R.M., Porter, D.A., Anwander, A., Feiweier, T., Calamante, F., Tournier, J.-D., Lohmann, G., Meyer, H., Knoesche, T.R., Turner, R., 2011. Whole-Brain, Multi-Shot, Diffusion-Weighted Imaging in Humans at 7T with 1 mm Isotropic Resolution. Proceedings of the 19th Annual Meeting of ISMRM, Montreal, Canada 541.

13 Holland, D., Kuperman, J.M., Dale, A.M., 2010. Efficient correction of inhomogeneous static magnetic field-induced distortion in Echo Planar Imaging. NeuroImage 50, 175-183.

14 Johansen-Berg, H., Behrens, T.E., 2006. Just pretty pictures? What diffusion tractography can add in clinical neuroscience. Curr Opin Neurol 19, 379-385.

15 Le Bihan, D., Mangin, J.F., Poupon, C., Clark, C.A., Pappata, S., Molko, N., Chabriat, H., 2001. Diffusion tensor imaging: concepts and applications. J Magn Reson Imaging 13, 534-546.

16 Mansfield, P., 1977. Multi-planar image formation using NMR spin echoes. J. Phys. C: Solid State Phys. 10, L55-58.

17 Miller, K.L., Pauly, J.M., 2003. Nonlinear phase correction for navigated diffusion imaging. Magn Reson Med 50, 343-353.

18 Mori, S., Zhang, J., 2006. Principles of diffusion tensor imaging and its applications to basic neuroscience research. Neuron 51, 527-539.

19 Nguyen, Q., Clemence, M., Thornton, J., Ordidge, R., 1999. Isotropic diffusion-weighted multishot imaging using automatic reacquisition.

Proceedings of the 7th Annual Meeting of ISMRM, Philadelphia, USA, 559.

20 Ordidge, R.J., Helpern, J.A., Qing, Z.X., Knight, R.A., Nagesh, V., 1994. Correction of motional artifacts in diffusion-weighted MR images using navigator echoes. Magn Reson Imaging 12, 455-460.

21 Porter, D.A., 2006. 2D-navigator-based re-acquisition for motion artefact suppression in multi-Shot, diffusion-weighted Imaging. Proceedings of the 14th Annual Meeting of ISMRM, Seattle, USA, 1047.

22 Porter, D.A., Heidemann, R., 2006. Multi-Shot, Diffusion-Weighted Imaging at 3T using readout-segmented EPI and GRAPPA. Proceedings of the 14th Annual Meeting of ISMRM, Seattle, USA, 1046.

23 Porter, D.A., Heidemann, R.M., 2009. High resolution diffusion-weighted imaging using readout-segmented echo-planar imaging, parallel imaging and a two-dimensional navigator-based reacquisition. Magn Reson Med 62, 468-475.

24 Porter, D.A., Mueller, E., 2004. Multi-shot diffusion-weighted EPI with readout mosaic segmentation and 2D navigator correction. Proceedings of the 12th Annual Meeting of ISMRM, Kyoto, Japan, 442.

25 Robson, M.D., Anderson, A.W., Gore, J.C., 1997. Diffusion-weighted multiple shot echo planar imaging of humans without navigation. Magn Reson Med 38, 82-88.

26 Schmierer, K., Wheeler-Kingshott, C.A.M., Boulby, P.A., Scaravilli, F., Altmann, D.R., Barker, G.J., Tofts, P.S., Miller, D.H., 2007. Diffusion tensor imaging of post mortem multiple sclerosis brain. NeuroImage 35, 467-477.

27 Schwartz, E.D., Duda, J., Shumsky, J.S., Cooper, E.T., Gee, J., 2005. Spinal cord diffusion tensor imaging and fiber tracking can identify white matter tract disruption and glial scar orientation following lateral funiculotomy. J Neurotrauma 22, 1388-1398.

28 Song, S.K., Sun, S.W., Ju, W.K., Lin, S.J., Cross, A.H., Neufeld, A.H., 2003. Diffusion tensor imaging detects and differentiates axon and myelin degeneration in mouse optic nerve after retinal ischemia. NeuroImage 20, 1714-1722.

29 Stejskal, E.O., Tanner, J.E., 1965. Spin Diffusion Measurements: Spin Echoes in the Presence of a Time-Dependent Field Gradient. J Chem Phys 42, 288-292.

30 Tournier, J.D., Calamante, F., Connelly, A., 2007. Robust determination of the fibre orientation distribution in diffusion MRI: non-negativity constrained super-resolved spherical deconvolution. NeuroImage 35, 1459-1472.

31 Turner, R., Le Bihan, D., 1990. Single-shot diffusion imaging at 2.0 Tesla. J Magn Reson 86, 445-452.

Contact
Julien Cohen-Adad, Ph.D.
Department of Electrical Engineering
Ecole Polytechnique de Montreal
2900 Edouard-Montpetit Bld.
Montreal, QC, H3T 1J4
Canada
Phone: +1 514-340-4711
Fax: +1 514-340-4611
jcohen@polymtl.ca